Magnetic resonance imaging (MRI) accoustic noise

Rizzo Sierra, Carlos Vicente

RIJKSUNIVERSITEIT GRONINGEN

Magnetic Resonance Imaging (MRI) acoustic noise:
Estimation, characterization and reduction

Proefschrift

ter verkrijging van het doctoraat in de
Wiskunde en Natuurwetenschappen
aan de Rijksuniversiteit Groningen
op gezag van de
Rector Magnificus, dr. F. Zwarts,
in het openbaar te verdedigen op
vrijdag 12 december 2008
om 14.45 uur

door

Carlos Vicente Rizzo Sierra
geboren op 24 november 1976
te Barrancabermeja, Colombia

Promotor:	Prof. dr. ir. H. Duifhuis
Beoordelingscommissie:	Prof. dr. L.P. Kok
	Prof. dr. V. Mellert
	Prof. dr. ir. N.B. Roozen

ISBN 978-90-367-3649-7 (Hardcopy)
ISBN 978-90-367-3648-0 (Online)

Paranimfen: Isa Valk (Absent)
Branislava Curcic-Blake

This work was funded partly by the University of Groningen (RuG) Ubbo Emmius Funds and partly by the Research School for Behavioral and Cognitive Neuroscience (BCN).

Printed and bound by MisEmpastes, in Bucaramanga, Colombia

Published by Bibliotheek der Rijks*universiteit* Groningen

Albert, during my brief existence (the most recent) imagination has proved to be equally important as knowledge, and their source proved to be curiosity. Therefore, for me "curiosity" is above imagination and knowledge. "Es en la adversidad que hallamos la fortaleza, en la enfermedad que apreciamos el valor de la salud, en el hambre que comprendemos el valor de los alimentos y en el agotamiento que valoramos la importancia del descanso". Een goed begin is het halve werk. We might be aware of our genes, but what about meme awareness? Please, know your memes.

To my curious parents and advisor

PREMISES

1. The acoustic noise generated during Magnetic Resonance Imaging (MRI) is a current concern because it reaches safety limits in many cases.

2. In order to effectively reduce this noise, a stronger multidisciplinary approach must be followed between hospital community (including patients), audiologists, industry and academia researchers.

3. Finding an ultimate noise reduction technique is not straightforward; every magnetic resonance (MR) scanner has its own acoustic transfer function characteristics and personalized sequences depending on its own software parameters.

4. Electro-acoustical MRI transfer function characterization combined with optimum sequence programming is very economical and effective in significantly reducing the MRI generated acoustic noise.

5. The combination of different noise reduction techniques applied simultaneously to the same MRI scanner facility (such as optimized pulse sequences, acoustic absorbing materials, new gradient coil designs, vacuum vessel enclosure and active vibration control) should lead to a large reduction in generated acoustic noise.

6. The future golden decade's hegemony of higher field MRI is uncertain, due to new improvements in the emerging technique of ultra low field MRI. The latter promises reduced costs, portability, quiet systems and broader coverage for patients.

CONTENTS

CHAPTER I.

INTRODUCTION

A Magnetic Resonance Imaging (MRI) scanner (figure 1) is a revolutionary device for three dimensional medical imaging of the internal structures (soft tissues), flow and other physiological phenomena in the human body (figure 2) and animals. Its great advantage is the non use of ionizating radiation, its non-invasive nature and higher spatial resolution, in the order of few millimeters. During functional imaging (fMRI) the machine is additionally used in brain mapping studies (figure 3). However, the interaction between the static magnetic field (figures 4 and 5) of this device and changing electrical currents in its gradient coils turns the scanner into a big loudspeaker. In detail, the gradient coil support system consists of a number of layers with composite materials, in which the copper gradient coils wires are submerged (1). The coils (figure 5) are driven by a sequence of pulse-like currents up to about 700 Amperes with frequency content mainly in the range of 100 - 3000 Hz. It is because of this switching current in the strong magnetic field, that dynamic Lorentz forces are generated in the gradient coils, resulting in vibration of the coils support system (2). This vibration causes direct sound radiation at the surface of the gradient coil system. Sound pressure levels above 120 dB are common for higher magnetic field scanners. This unwanted noise causes distraction, anxiety, results in (auditory) brain stimulation not related to the task at hand, and possibly hearing damage (3-7).

Figure 1. The MRI scanner facility. Courtesy of Anita Kuiper.

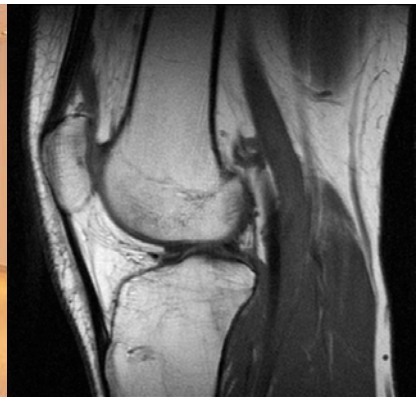

Figure 2. One anatomical MRI image of the knee. Courtesy of Wikipedia.

Nowadays, there is a tendency to enable the use of surgical intervention techniques during the MRI scanner process. This implies the presence of a team of physicians and assistants inside the scanner room in addition to the patient subject. Additionally, it poses a complicating factor since these techniques require fast scanning sequences which result in a higher noise load for those inside the scanner room. Therefore, many methods of MRI acoustic noise reduction have been proposed such as active noise cancellation (8), destructive sound interference in gradient coil design (9), and sound attenuation by vacuum layers (10).

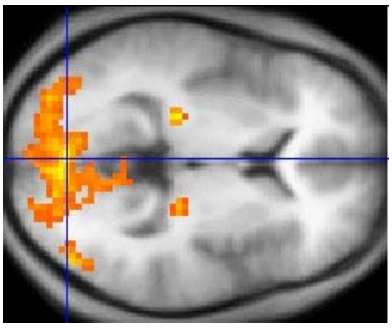

Figure 3. One fMRI image showing regions of activation in orange, including primary visual cortex. Courtesy of Wikipedia.

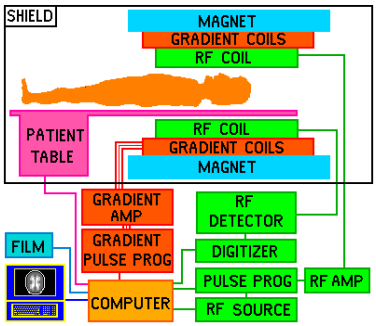

Figure 4. Overview of MRI hardware. Courtesy of J.P. Hornak, The Basics of MRI.

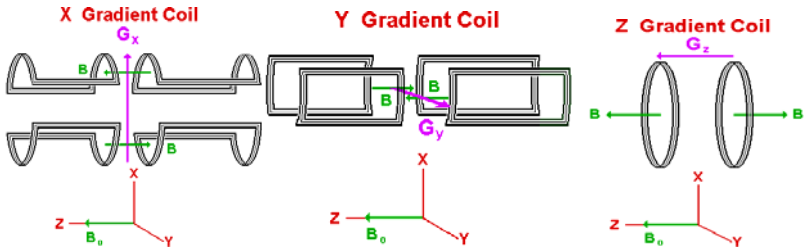

Figure 5. The Three MRI gradient coils imposing a varying (gradient) magnetic field for each direction (G_X , G_Y and G_Z) in the static magnetic field B_O in order to make images. Courtesy of J.P. Hornak, The Basics of MRI.

Moreover, it has been proposed (11) that the physical structure of the MR scanner behaves as a linear time invariant (LTI) electro-acoustical system, where gradient coil currents $I(t)$ can be interpreted as input and the generated sound pressure signals $p(t)$ as outputs of the LTI-system. This leads to a MRI electro-acoustical transfer function concept that characterizes the system and is a first step in modeling and predicting MRI acoustic noise. Additionally, by avoiding gradient coil system resonance frequencies the scanner experiences a substantial acoustic noise reduction (12).

The so-called linear time invariant system approach to characterize, model and predict the MRI acoustic noise is discussed and the results shown in **chapter 2** for one MRI facility. The estimation of the system damping properties is also shown. In addition, a new physical interpretation of noise generation is introduced by using the derivative of the input in the electro-acoustical transfer function classical estimation. Another noise reduction technique relies on pulse sequence optimization recently referred as silent imaging (13, 14). The pulse sequence controls the electric gradient currents and they define the way in which the magnetic field is changed to obtain location information. When scanning starts, the pulse sequence is known since they depend on scanning parameters like repetition time (TR), echo time (TE), and the field of view (FOV) (15). Adjustments of these parameters affect the gradient currents, in time as well as spectrum. It has been also shown to some extent that the vibrations

arising from the gradient currents contain similar frequencies as the gradient currents. Therefore, **chapter 3** describes and presents results on how the physical interpretation introduced in chapter one can be used in acoustic noise reduction by optimizing pulse sequences for one MRI facility. The new acoustic noise reduction is achieved by timing the ramps of the trapezoids (currents) such that two resonance frequencies of the MR scanner gradient coil transfer function are eliminated. Zeros in the gradient current spectrum can be set to selected frequencies, such as the two most prominent resonance frequencies in the gradient coil transfer function. In addition, a Lorentz force model of a gradient coil is developed to further show the relation between the time derivative of the gradient input currents and the generated MRI sound.

Typical functional MRI acoustic noise has very special time waveform characteristics such as its impulsive nature and amplitude modulated carrier (16). Even though, scientific studies report fMRI acoustic noise in current scales such as sound pressure level (SPL) in dB, dB(A), equivalent continuous noise level (L_{eq}), and peak levels (L_{pk}); there is no accepted acoustical standard with a proper physical or subjective loudness scale for this type of impulse noise. Accordingly, **chapter 4** attempts to cover this gap by obtaining a subjective measure of fMRI scanner noise loudness using a psychophysical experiment, and comparing it to its current physical measure using sound pressure levels for echo planar imaging (EPI) based scanner noise. Attempts to correlate both (subjective and current physical) fMRI acoustic noise loudness measures should lead to a better estimation, characterization and understanding of the effect of this type of noise in the human ear; also could elucidate a proper loudness scale related to this type of noise and eventually lead to its perceived reduction. Although, MRI electro-acoustical transfer function characterization (discussed in chapter 1 and 2) was proposed in the late 90's (11), there is no study assessing the variability of that estimation inside and outside the scanner bore, that is assessing the effects of the MRI bore enclosure. Then, **chapter 5** aims to estimate enclosure effects in this transfer function main resonance peaks by computing transfer function in a total of 6 locations along the operator room direction, three locations inside and three outside the bore. The idea that acoustic reverberation plays a role in MRI electro-acoustical

transfer function is also investigated by overall reverberation time estimation for the same locations.

Finalizing this work, **chapter 6** presents a summary of the four studies mentioned above, whereas, the general conclusions and future prospects are discussed in **chapter 7**.

REFERENCES

1. Kuijpers AH. Acoustic modeling and design of MRI scanners. PhD thesis. Technical University Eindhoven. 1999.

2. Hurwitz R, Lane SR, Bell RA, Brant-Zawadzki MN. Acoustic analysis of gradient-coil noise in MR imaging. Radiology 1989;173(2):545-548.

3. Bandettini PA, Jesmanowicz A, Van Kylen J, Birn RM, Hyde JS. Functional MRI of brain activation induced by scanner acoustic noise. Magn Reson Med 1998;39(3):410-416.

4. Brummett RE, Talbot JM, Charuhas P. Potential hearing loss resulting from MR imaging. Radiology 1988;169(2):539-540.

5. Cho Z, Chung S, Lim D, Wong E. Effects of the acoustic noise of the gradient systems on fMRI : A study on auditory, motor and visual cortices. 39 ed. 1998. 331-335.

6. Elliott MR, Bowtell RW, Morris PG. The effect of scanner sound in visual, motor, and auditory functional MRI. Magn Reson Med 1999;41(6):1230-1235.

7. Mazard A, Mazoyer B, Etard O, Tzourio-Mazoyer N, Kosslyn SM, Mellet E. Impact of fMRI acoustic noise on the functional anatomy of visual mental imagery. J Cogn Neurosci 2002;14(2):172-186.

8. McJury M, Stewart RW, Crawford D, Toma E. The use of active noise control (ANC) to reduce acoustic noise generated during MRI scanning: some initial results. Magn Reson Imaging 1997;15(3):319-322.

9. Mansfield P, Haywood B. Principles of active acoustic control in gradient coil design. MAGMA 2000;10(2):147-151.

10. Katsunuma A, Takamori H, Sakakura Y, Hamamura Y, Ogo Y, Katayama R. Quiet MRI with novel acoustic noise reduction. MAGMA 2002;13(3):139-144.

11. Hedeen RA, Edelstein WA. Characterization and prediction of gradient acoustic noise in MR imagers. Magn Reson Med 1997;37(1):7-10.

12. Tomasi DG, Ernst T. Echo planar imaging at 4 Tesla with minimum acoustic noise. Journal of Magnetic Resonance Imaging 2003;18(1):128-130.

13. Hennel F, Girard F, Loenneker T. "Silent" MRI with soft gradient pulses. Magn Reson Med 1999;42(1):6-10.

14. Hennel F. Fast spin echo and fast gradient echo MRI with low acoustic noise. J Magn Reson Imaging 2001;13(6):960-966.

15. Hoiting GJ. "Measuring MRI noise". PhD Thesis, 2005. ISBN 90-367-2235-7 (Online version).

16. Counter SA, Olofsson A, Borg E, Bjelke B, Haggstrom A, Grahn HF. Analysis of magnetic resonance imaging acoustic noise generated by a 4.7 T experimental system. Acta Otolaryngol 2000;120(6):739-743.

CHAPTER II.

ACOUSTIC fMRI NOISE: LINEAR TIME INVARIANT SYSTEM MODEL[1]

Carlos V. Rizzo S, Maarten J. Versluis, Johannes M. Hoogduin and Hendrikus Duifhuis

—Functional magnetic resonance imaging (fMRI) enables sites of brain activation to be localized in human subjects. For auditory system studies, however, the acoustic noise generated by the scanner tends to interfere with the assessments of this activation. Understanding and modeling fMRI acoustic noise is a useful step to its reduction. To study acoustic noise the MR scanner is modeled as a linear electro-acoustical system generating sound pressure signals proportional to the time derivative of the input gradient currents. The transfer function of one MR scanner is determined for two different input specifications: (1) by using the gradient waveform calculated by the scanner software, and (2) by using a recording of the gradient current. Up to 4 kHz the first method is shown as reliable as the second one, and its use is encouraged when direct measurements of gradient currents are not possible. Additionally, the linear order and average damping properties of the gradient coil system are determined by impulse response analysis. Since fMRI is often based on echo planar imaging (EPI) sequences, a useful validation of the transfer function prediction ability can be obtained by calculating the acoustic output for the EPI sequence. We found a predicted sound pressure level (SPL) for the EPI sequence of 104 decibels (dB) SPL compared to a measured value 102 dB SPL. As yet, the predicted EPI pressure waveform shows similarity as well as some differences with the directly measured EPI pressure waveform.
Index Terms—acoustic noise, fMRI, gradient noise, linear system, SPL.

[1] Published in modified version: IEEE Transactions on Biomedical Engineering, Vol. 55 No. 9, September 2008.

I. INTRODUCTION

FUNCTIONAL magnetic resonance imaging (fMRI) has successfully become an essential tool in human brain imaging since first proposed in 1990 (1, 2). But functional magnetic resonance imaging acoustic noise is a concern for the medical imaging and engineering community, since it exposes volunteers, patients, operators and medical practitioners to doses of high level sound for periods of time in the order of hours[2]. Effects of this airborne sound exposure range from potential hearing loss to nonlinear effects on brain activation in patients and volunteers (3-7). Even though for the latter there are timing modifications in image acquisition, such as sparse sampling, (8-10) aimed at reducing the influence of noise on brain activity, they are not generally applied because they compromise data acquisition efficiency. Also, earplugs or other protectors which are worn by subjects (11) are not sufficient to achieve acceptable quiet conditions (12, 13).

The mechanism and process that produces the gradient magnetic field is the primary source of this noise. That is, the gradient coils that use strong currents within the static background magnetic field, create Lorentz forces as detailed in (14). These currents are necessary to produce the spatially and temporally varying magnetic fields required for imaging. In previous studies (15, 16) of the acoustic scanner noise it has been proposed that the physical structure of the MR scanner behaves as a linear time invariant (LTI) electro-acoustical system where gradient coil currents $I(t)$ can be interpreted as input and generated sound pressure signals $p(t)$ as outputs of the LTI-system. Physically, the system is made of the mechanical structure of the MR scanner, including magnet, gradient coils, RF body coil, support structures and the structure of the acoustic space inside the body coil where the patient would typically be exposed to the noise. The assumption that the scanner noise follows linear time invariant (LTI) system properties goes back to 1997 (15). Experimental application and verification of this assumption, however, remains scarce. In a

[2] Note that for regular MRI less or similar sound levels apply, but in that case the exposure duration is greatly reduced.

short letter (16) this approach is explicitly advocated, and in studies (17) and (18) the first attempts of such an analysis have been reported. Following this LTI approach, the ratio of output and input spectra defines the classical electro-acoustical transfer function (19) $H(f)$ of this system**.**

A good number of studies (15, 20-24) deals with just acoustic noise measurements during conventional anatomical MRI. Hedeen et al (15) expanded the analysis and reported that acoustic noise signatures were associated with gradient pulse waveforms. They proposed that a common transfer function consistently relates the acoustic noise responses to the gradient currents.

A second group of studies deals with acoustic noise measurements during functional MRI (25-29). Here we also focus on the sound produced in fMRI studies. Since almost all of these studies use echo planar imaging (EPI) sequences (2, 30) which imply the choice of rapid gradient switching, the generation of high level acoustic noise (25, 31) is a straightforward consequence. This study models single shot gradient-echo EPI (2) acoustic noise using LTI system theory. Therefore, our model attempts to characterize and predict this noise by:

1) estimation of the MRI electro-acoustical transfer functions for each gradient coil using pulses as inputs (both as software gradient waveform and as recorded gradient current),
2) estimation of decay times (32, 33) of the acoustic responses[3], which are largely determined by damping properties of the gradient coil system,
3) prediction of sound pressure waveform and spectrum generated by one typical EPI sequence.

[3] The decay time τ is the time constant parameter of the exponentially decaying asymptote $e^{-t/\tau}$ that matches the acoustic (im)pulse response. Its reciprocal value $\sigma(=1/\tau)$ is called damping factor or temporal absorption coefficient. Another related quantity is the reverberation time, defined as the time over which the (asymptotic) response decays by 60 dB (32, 33).

II. MATERIAL AND METHODS

The experiment was performed on a Philips Intera 3 Tesla MR scanner [maximum gradient strength 21 milliTesla(mT)/meter(m)] per axis, located at the Behavioral and Cognitive Neurosciences (BCN) NeuroImaging Center (NiC) at the University of Groningen, The Netherlands. We employed a non-magnetic microphone support specially fitted to the edges of the patient's table inside the imager bore. Since the patient's table is indirectly coupled to the housing, the gradient coil cylinder is not directly coupled to the patient's table. Therefore, we expect that vibration cross-talk is limited to less than 1 dB. This was tested by measuring the sound field directly outside the bore. A more precise verification of this point requires simultaneous vibration measurement of the microphone housing, and is recommended for future research. To record sound inside the scanner a 1/2 inch condenser microphone Bruel Kjaer (B&K) 4190 (tested for MRI in (34)) was mounted on a non magnetic specially designed support and connected to a preamplifier (B&K ZC0026). Before measurements microphone and preamplifier were calibrated using sound level calibrator 4230 [B&K, ~94 dB at 1000 Hertz (Hz)]. This microphone and preamplifier are connected to a B&K Modular Precision Sound Analyzer 2260 through a 10 meter long extension cable (B&K AO0442). The 3T scanner used in this study supports a maximum current amplitude of approximately 700 Amperes (A), which can be read out using a manufacturer provided current monitor signal of 10 Volts (V), that is, 10V ≡ 700A, for each gradient coil. Acquisition of the scanner gradient current monitor signal and of the microphone signal takes place via a 16 bits digital acquisition board (National Instruments 6052E) using LABVIEW 6.0 software (National Instruments 2000). Since no radio frequency (RF) signals are used for these measurements, a phantom was not needed, and the receiver RF head coil was removed from the scanner. All analog signals are low-pass filtered (Kemo Inc., 8-pole Bessel, cut-off frequency 14 kHz) before acquisition and are sampled at 100 kHz; the EPI set is sampled at 50 kHz. The data were analyzed using the MATLAB signal analysis toolbox (R2006a).

Two input sequences were recorded with the generated output sound, while the helium coolant pump for the imager's permanent magnet was turned off. First a calibration trapezoidal pulse [0.1 milliseconds

(ms) raise and fall time, 0.01 ms plateau time, 10 mT/m amplitude] was presented to the X-gradient coil at 0.5 seconds (s) intervals for 10 seconds. This procedure was repeated for Y and Z gradients. The second sequence was used for model validation and consisted of EPI signals on the gradient coils (slice selection gradient was chosen in the static magnetic field direction Z, whereas phase and frequency encoding were chosen in X and Y perpendicular directions). The EPI parameters were: 3 seconds repetition time, 35 ms echo time, 46 slices, 64x64 matrix, field of view 224 millimeters (mm) and dominant frequency readout train of 925 Hz. Recordings were performed for 20 seconds. Additionally, 10 seconds of background noise (air-handling system) was recorded for reference. All sound pressure recordings reported here were carried out at the scanner isocenter, which approximates the location where a human ear would be during scanning thereby giving an indication of the patient ear exposure. The non-magnetic microphone support fitted to the edges of the patient's table inside the imager bore. It kept the microphone in a rigid horizontal position within a 1 mm range at the scanner isocenter. The input gradient currents for calibration pulses and test EPI signals were recorded by the acquisition system. Sound pressure waveforms generated by calibration and test signals, were derived from the recorded microphone output waveform using the microphone sensitivity [48.6 milliVolts(mV)/Pascal(Pa)].

From the different excitation methods that can be used to estimate the MR scanner transfer function, such as broadband noise, pulses, and frequency sweeps, we selected the pulse excitation method. The transfer function is determined for two different input specifications: by using the theoretical gradient waveform calculated by the scanner software, and by using an experimental recording of the generated gradient current (as explained before). Calculated gradient waveforms were generated by the scanner's software based on the selected sequence and acted as an input for the gradient amplifier. Using the manufacturer provided conversion factor (1V $\equiv$ 70 A and 1 milliT/m $\equiv$28.4 A), the gradient current was calculated from this input signal. The calculated gradient coil current is not exactly identical to the measured gradient coil current since no eddy current compensations are taken into account in the calculated gradient waveforms. It is noted that the step of measuring and recording gradient coil currents takes experimental scanner time for the calibration and specific tools for the

measurement, which imply specific costs. Both electro-acoustical transfer functions (based on calculated gradient coil currents, and based on recorded gradient coils) are estimated following the same procedure (and using same output pressure). Their magnitude squared coherence function (35) was estimated from their complex functions to quantify the degree of similarity.

So far, gradient current has been chosen as the relevant input signal for the MR electro-acoustical transfer function. The reported transfer functions in literature (standard: pressure over input gradient current) show flat spectra up to the highest frequencies (f), which we did not expect because physically realizable systems must have a high-frequency (hf) asymptote that falls off [4]. Therefore, we propose to take the time derivative of $I(t)$, $\frac{\partial I(t)}{\partial t}$, as the input signal for the electro-acoustical transfer function of this system, $H'(f)$. This transfer function relates to the classical one by just a factor $H'(f) = \frac{H(f)}{2\pi j f}$.

From the recorded train of 20 stimulus pulses with the acoustic responses for the X, Y and Z gradients, the second stimulus (current) pulse, located at 0.5 s is taken as representative example. Its amplitude spectrum per gradient is computed after application of a 0.5 s Kaiser window centered at the stimulus peak, and with Kaiser window parameter β = 11 (36). The acoustic response of each representative pulse is band-pass filtered in the auditory range (20 Hz to 20 kHz) by means of a 2nd order Butterworth digital filter (sampling frequency 50 kHz, 25000 sample points, cutoff frequency 6 Hz). The amplitude spectrum of each representative pulse is computed with application of the specified Kaiser window. A 10 s background signal is also filtered within the auditory range and exponentially time averaged (37) (using 125 ms time constant equivalent to the Fast (F) sound level meter settings which use a resistor-capacitor RC time of 125 ms) over 0.5 s

[4] A horizontal *hf* -asymptote can occur only for the trivial delta-function impulse response. Any causal response that is longer will have a *hf* boundary, amongst others because it has a finite power.

samples. The sample with maximum root-mean-square (RMS) pressure is taken and its amplitude spectrum is estimated after applying the Kaiser window specified above.

Given the response pressure (in Pa) and the time derivative of the stimulus input current (in A/s), the transfer function (19) is computed for each gradient coil taking the (complex) ratio of response spectrum over input spectrum. This is computed for each pulse and then averaged across 19 pulses. Again, a 0.5 s Kaiser window (β =11) centered at the stimulus peak, was used for optimal processing of stimuli and responses. In the present study the pulse excitation up to 8 kHz (see figure 1 bottom) was used to estimate the transfer function. The obtained transfer functions were then used to compute the predicted EPI frequency spectrum by adding up the results for each gradient, as described next:

$$P(f) = H'_X(f)G'_X(f) + H'_Y(f)G'_Y(f) + H'_Z(f)G'_Z(f) \qquad (1)$$

where $P(f)$ is the predicted EPI frequency spectrum; $H'_X(f)$, $H'_Y(f)$ and $H'_Z(f)$ are the X, Y, and Z gradient transfer functions, respectively; $G'_X(f)$, $G'_Y(f)$, and $G'_Z(f)$ are frequency spectra of EPI X, Y and Z gradient current derivatives, respectively, that is, $G'_X(f) = FT\{\frac{\partial}{\partial t} FT^{-1}\{G_X(f)\}\} = j2\pi f G_X(f)$, etc.

Frequency spectra for the measured EPI acoustic waveforms and EPI input current derivatives are calculated individually by averaging 5 subsequent sections of 0.5 seconds (3 s apart, and using 0.5 s Kaiser windows, β =11) starting at 1.5 s (see figures 5 A-G, and 6 top). The overall SPL (ANSI S1.13-1995 (R1999)) for the EPI noise, both predicted and measured, was calculated over 0.5 s from the sound pressure spectrum (in Pa/Hz) using its RMS amplitude spectrum (33), integrating positive frequencies up to Nyquist frequency (25 kHz) and using the appropriate bandwidth correction for the employed Kaiser windows. Equation (1) defines the (predicted) complex sound pressure spectrum $P(f)$. Its absolute value represents the predicted sound pressure amplitude spectrum, and its inverse Fourier transform shows the EPI predicted sound pressure waveform. The measured EPI (0.5 s windowed) waveform depicted in figure 7 (bottom) is found by

inverse Fourier transform of the measured EPI Fourier spectrum averaged over 7 repetitions. The time constant τ (32, 33), is estimated by curve fitting the impulse response envelope (per gradient coil) to the function $\alpha t e^{-t/\tau}$, which involves also a scaling factor α, and the linear term t (build up approximation). The asymptotic amplitude envelope decay was obtained from the linear approximation of the absolute value of the impulse response on a logarithmic (dB) scale. For each gradient coil the impulse response is approximated by $\alpha_i t e^{-t/\tau} \Sigma_i \sin(2\pi f_i t)$ where the f_i represent the three frequencies with highest transfer function gain. The total gradient coil system is approximated by a sum of the frequencies with the highest gain for each gradient. The real impulse response is obtained by inverse fast Fourier transform of the X, Y and Z transfer functions over the 500 Hz to 8000 Hz range.

III. RESULTS

Figure 1 (top) shows 3 out of 20 stimulus pulses (Y gradient), with their acoustic responses, used for calibration. The amplitude spectrum of the representative Y gradient input pulse located at 0.5 s is shown in figure 1 bottom. The amplitude spectra of the acoustic responses (per gradient) to this pulse are given in figure 2 (on a linear frequency scale). This figure also shows background spectra up to approximately 500 Hz which show levels that are comparable to the acoustic responses. This implies that the signal to noise (S/N) ratio in this low-frequency range prohibits reliable estimates of the transfer function. Above 500 Hz the S/N ratio increases, and spectral estimation becomes increasingly significant. The estimated transfer function gain per gradient is shown in figure 3 (on a logarithmic frequency scale), and shows high-frequency asymptotes falling off with $1/f$. The top three (figure 3) show different transfer functions based on recording of the gradient current, whereas, the one at the bottom shows the transfer function (Z gradient) based on gradient waveform calculated by the scanner software. In figure 3 bottom we compare (for Z gradient only), the recorded and calculated scanner transfer functions.

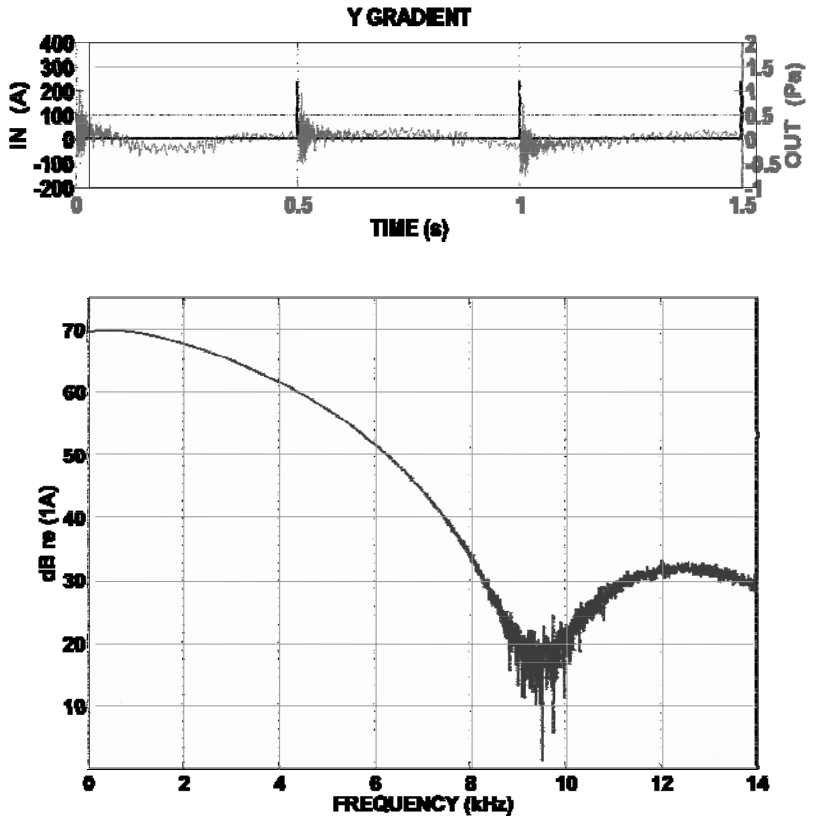

FIG. 1. Top: Input train of pulses (Dark grey) and output acoustic response (light grey) Y gradient. Bottom: Pulse amplitude spectrum Y gradient.

They appear to be identical over the 500 Hz to 3000 Hz range, where their magnitude squared coherence was found to be very close to 1 (deviation <0.001). Very similar results were obtained for the X and Y gradients. However, it should be noted that the "recorded" gradient coil current is not exactly identical to the "calculated" current (based on the generated value by scanner software). This is due mainly to eddy current compensations not taken into account in the second case.

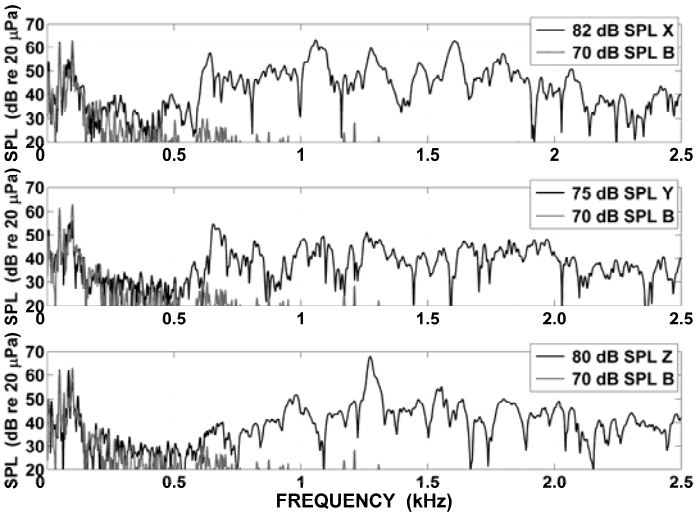

FIG. 2. Pulse (representative) acoustic response amplitude spectra per gradient (above in dark: X, Y, Z) and background signal (below in gray: B).

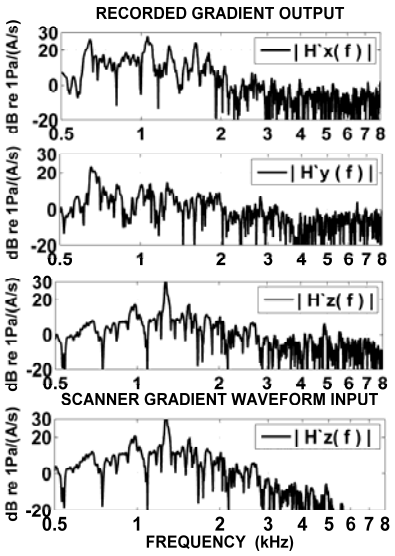

FIG. 3. X, Y and Z Transfer function gain. Top 3: By using a recording of the gradient current. Bottom: By using the gradient waveform calculated by the scanner software.

The X gradient coil transfer function presents the highest gains at 1058 Hz (28 dB), 642 Hz (26 dB), 1606 Hz (25 dB). The Y transfer function presents maximum gains at: 654 Hz (23 dB), 1260 Hz (15 dB) and 1088 Hz (14 dB). Finally, the Z transfer function presents peaks at 1274 Hz (32 dB), 1554 Hz (18 dB) and 982 Hz (17 dB). Note that expected similarity between resonance modes for the X and Y gradient coils leads to expectation of similarity between the peaks in the X and Y spectra, which is observed only in part. The images in figure 4 A-C show the impulse responses (dark) and obtained amplitude envelopes (dotted) of the X, Y and Z gradients. It was found that the X and Z gradient coils were slightly less reverberant or more damped than the Y gradient coil, as follows from the estimates of the time constants: τ_x = 11 ms, τ_y = 13 ms, and τ_z = 11 ms. The proposed approximation by superposition of third order linear systems with impulse responses $\alpha_i t e^{-t/\tau} \Sigma_i \sin(2\pi f_i t)$, applying the parameter values given above, is shown in figure 4 D for the Y gradient.

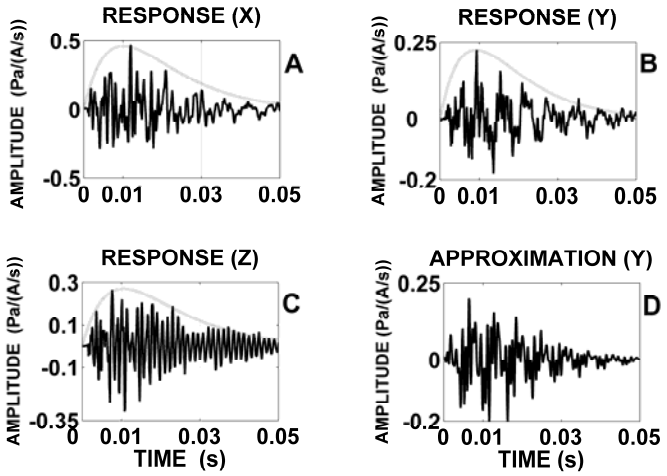

FIG. 4. Impulse responses (dark line) of X, Y and Z gradient coils displaying estimated envelopes (dotted line), in A, B, and C respectively: $120te^{-88t}, 50te^{-75t}$ and $85te^{-88t}$. D: (dark line) Approximation of Y gradient coil behavior by superposition of third order linear systems with impulse response $\alpha_i t e^{-\sigma t} \Sigma_i \sin(2\pi f_i t)$.

The EPI input signals per gradient coil and measured EPI acoustic waveform (repetition time 3 s) are shown in figure 5 (D to F is zoom from A to C, G is EPI acoustic waveform). The presented input currents show a periodicity of 53 ms (slice selection), which also appears in the EPI acoustic waveform (figure 5 G). The phase encoding gradient $G_x(t)$ is a trapezoidal periodic signal of 1824 Hz plus two short pulses (at onset and offset), shown in figure 5 A. The frequency encoding gradient $G_y(t)$ shows a trapezoidal periodic signal of 912 Hz, which represents the readout frequency. Additionally, a common periodicity of approximately 19 Hz between two successive frequency peaks is found in each signal from figure 6 and 7. This is to be related to the 53 ms acquisition time per slice, represented as the time periodicity for each signal shown in figure 5 A,B,C & G.

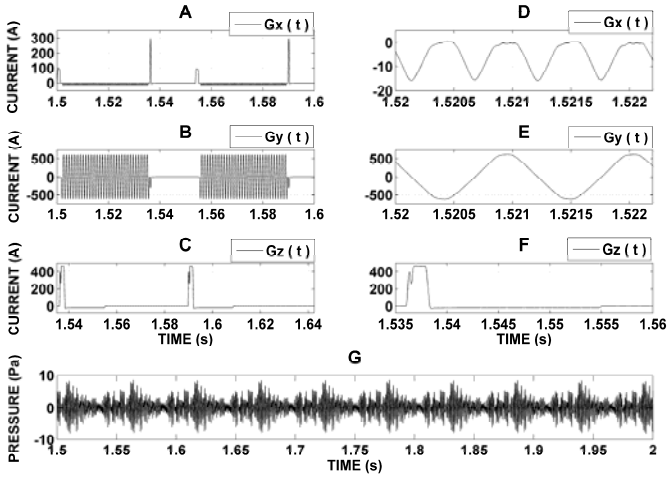

FIG. 5. EPI simultaneous input current signals per gradient. D to F is zoom from A to C respectively. G: Measured EPI acoustic waveform.

The LTI-system MRI-model prediction (using fig 3 top three transfer functions: X, Y and Z simultaneously as described in equation 1 page 16) for EPI acoustic noise (104 dB SPL) is found 2 dB above measured EPI noise (102 dB SPL). Figure 6 shows that predicted (B) and measured (A) EPI amplitude spectra resemble each other roughly, even at the highest frequency peaks above 4 kHz. As shown in figure 6 A and B, the highest EPI peak in the spectra is at about 920 Hz (both

labelled with number 1). The higher harmonics of this fundamental frequency are shown in the predicted and measured EPI amplitude spectra in figure 6. It is noted that the even harmonics present in the measured EPI amplitude spectrum (figure 6 A) correspond to the peaks in the X-gradient input current spectrum (figure 6 C), and that the odd harmonics present in the EPI amplitude spectrum correspond to the peaks in the Y-gradient input current spectrum (figure 6 D).

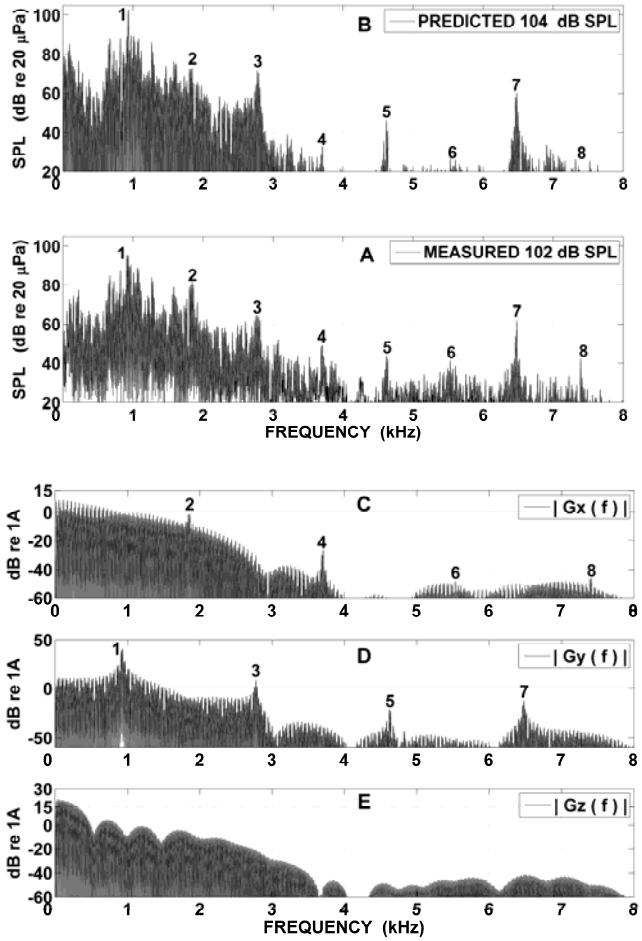

FIG. 6. Measured (A) and predicted (B) EPI amplitude spectrum. C-E: Amplitude spectrum for EPI input current per gradient (Phase encoding, frequency encoding and slice selection respectively).

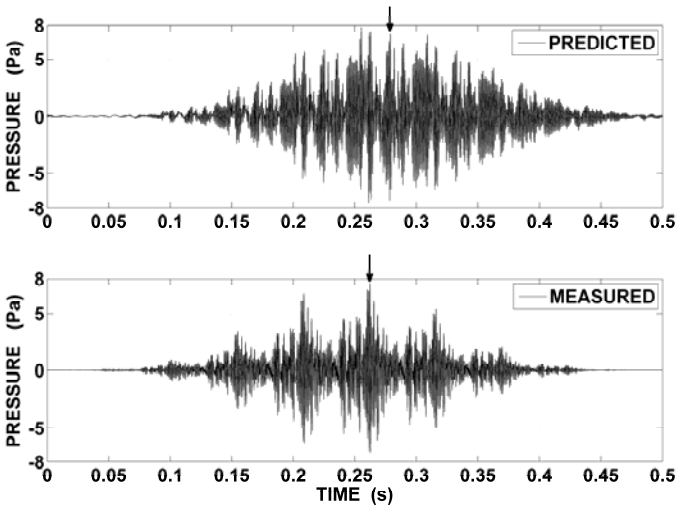

FIG. 7. Top: Predicted 0.5 s. windowed EPI acoustic waveform. Bottom: 0.5 s. windowed measured EPI acoustic waveform.

The measured spectrum shows in particular noticeably stronger even order harmonics than the predicted spectrum, whereas, the predicted EPI amplitude spectrum seems to overstate the effect of the frequency encoding gradient (odd harmonics). The predicted EPI waveform (figure 7) appears to be delayed by approximately 20 ms compared to the measured signal (this is probably largely due to differences in triggering details for calibration and EPI application), and also its fine structure is not fully recovered.

IV. DISCUSSION

In principle, all resonance modes of the gradient coil cylinder, as well as all other coupled mechanical or acoustical resonance modes, are excited by broadband signals, such as short pulses. Similarity between X and Y coil structures provide a basis for similarity between the X and Y gradient responses. Transfer function and impulse response estimations for the gradient coil system (figures 3 and 4) show that the gradient coil systems can be approximated by a superposition of third order linear systems with impulse response: $\alpha_i t e^{-t/\tau} \Sigma_i \sin(2\pi f_i t)$.

Here the f_i represent the three resonance frequencies with highest transfer function gain per gradient coil (see figure 4 D). The time constant τ of the system was estimated to be about 1/100 s (for all directions), which is equivalent to a damping factor in the 100 s^{-1} range. Tomasi et al (38) measure a vibration impulse response using three piezoelectric transducers. Our acoustical impulse response differs from their vibration impulse responses in few characteristics: our responses shows a build up time of approximately 10 ms where the peak is located. Additionally, their response lacks strong low frequency components, which are observable in our response, especially in the X and Y gradient coils. Their time constants (8 ms for X and Y, 13 ms for Z) are comparable to our values (11 ms, 13 ms and 11 ms, respectively). Recently Tomasi et al (39) formulated a simple theory for vibration of MRI gradient coils. They show a vibration impulse response of the three gradient coils elicited by excitation in the longitudinal Z direction coil only. Their overall shape looks somewhat similar to our acoustic impulse responses even though they employed a different MR scanner and a different sensor (piezoelectric).

If the slice selection gradient is chosen in the static magnetic field direction Z, and phase and frequency encoding are chosen in X and Y perpendicular directions, then the phase encoding X-gradient in figure 6 C can be mainly responsible for the even harmonics and broadband spectrum (due to two pulses of 0.35 ms and 1.4 ms duration, figure 5 A). The frequency encoding Y-gradient in figure 6 D is responsible for the odd harmonics and non harmonics. Finally, the slice selection or Z-gradient in figure 6 E is responsible for more broadband spectrum in total pressure spectrum (figure 6 A,B), mainly due to the 2 ms pulses (figure 5 C, F).

Recently More et al. (18) showed an EPI noise LTI model of their 4T scanner facility. Their gradient coils were calibrated with various input pulse amplitudes and it was suggested that they behaved linearly above 300 Hz. Three types of sound pressure response were reported in their noise characterization: harmonic, nonharmonic and broadband components. Also the independent contribution of the gradient coils to these three types of sound pressure responses is discussed. Their predicted and measured EPI spectra were compared qualitatively only.

Although the results from some studies (29, 40) were pointing towards an independent contribution of gradient coil spectrum to total EPI pressure spectrum, More et al. (18) were the first to clearly show and explain this relationship, which we now have collaborated in our study. Our findings match their study rather closely, even though they used a 4T MRI scanner with a head RF coil and humanoid dummy, and three different locations for microphone recordings.

Although the main static magnetic field direction is by convention always aligned along the Z-axis, this is seldom the precise direction of the slice selection gradient after placing a subject inside the scanner. Usually an oblique angle between the main magnetic field direction and the slice selection gradient is applied. Therefore, phase and frequency encoding gradients are not always in the precise X, Y directions. The implication is that slice selection and readout gradients will be combinations of at least two gradient fields created by their specific gradient coils. We want to point out that all literature studies referenced dealing with measured, analyzed, predicted and/or modeled MRI acoustic noise, appear to tacitly assume that slice selection, phase and frequency encoding for the scanner are precisely in the Z, X and Y directions. However, this is not usually the case. In fact we made the same simplifying assumption but we also shortly discussed the general case.

Cho et al. (26) found many equally intense discrete frequency peaks spread throughout the spectrum for a 1.5T scanner, whereas, Miyati et al. (25) presented the EPI noise spectrum in octave bands that peaked in the 2 kHz band. For a 3T scanner, Wessinger et al. (27) found a dominant frequency at 2.5 kHz. Counter et al. (28) found amplitude modulated pulse envelopes and multi-peaked spectra in EPI based noise. But, none of these studies (25-28) commented on the relationship between these dominant noise frequencies and the gradient activity in their imaging pulse sequence. More detailed studies performing EPI noise analysis include (29) and (40). Ravicz et al (29) found that acoustic noise waveforms depend on the frequency encoding gradients of the imaging sequences used. They found that the amplitude of the acoustic noise waveform was mainly attributable to the gradient coils assembly. Their EPI noise spectra presented a harmonic structure in which the first peak coincides with fundamental frequency of the readout gradient, and harmonics fall off at more than

12 dB/oct. On the other hand, Li et al. (40) present three modes for the first dominant harmonic during the frequency encoding gradient generating acoustic noise with expected harmonic behavior. Even though a low-mode EPI gradient input spectrum is shown, the only comment on possible specific contributions of gradient coils to the EPI sound pressure spectrum was that the Y-gradient is dominant. They estimated the MRI transfer function by using sinusoidal sweep excitations on the Y-gradient coil only.

Differences between the predicted and measured acoustic EPI amplitude spectra (figure 6 A, B) and EPI waveforms (figure 7), probably can be attributed to the time delay between triggering differences for calibration and validation signals (estimated in the order of 20 ms). Additional differences must be due to limitations of the current model. The scanner consists of many components that are coupled and can interact both linearly and nonlinearly. Moreover, additional contributors to acoustic MR noise are the eddy current induced vibrations in metal structures such as the cryostat inner bore, and the vibration in the RF body coil (for example suggested in (41) and (42)), which can contain (nonlinear) clipping. The results shown in figure 6 suggest that the measured EPI amplitude spectrum can be understood as a superposition of harmonic, non harmonic and broad band components. In all studies mentioned here the SPLs produced by EPI sequences were computed through linear electro-acoustical modeling. This method is also valuable for MR acoustic control applications (43-47), including MRI active noise cancellation (48). However, none of the studies discussed here performed EPI waveform reconstruction nor attempted to estimate it. Hence, so far current electro-acoustical modeling appears to give an appropriate prediction of EPI sound pressure levels, but it still has a limited precision in time domain reconstructions. For existing MRI scanners, another technique that can substantially reduced the acoustic noise employs the so-called silent sequences. Three of the rules for this silent imaging (49) are: (1) the gradient waveform should have sinusoidal gradient slopes at frequencies that avoid peaks in the transfer function (resonances), (2) use maximum slope duration, and (3) use a minimum number of slopes. Later, it was shown that this method could be improved by removing all plateaus in the gradient waveform, and use purely sinusoidal gradient waveforms (50). Comparing the resulting image quality with standard pulse sequences yields only minor differences,

whereas the acoustic noise is reduced significantly, and functional imaging with this technique is possible (51, 52). The blood oxygenation level dependent (BOLD) response can be measured but needs a long imaging time and is therefore more sensitive to scanner drift.

We showed for the examined MR scanner that the acoustic response of the gradient coil system is proportional to the time derivative of the input gradient current. This is formalized in the adopted transfer function $H'(f) = \frac{H(f)}{2\pi j f}$. This new interpretation supports the results by Hennel et al. (49, 50) suggesting that optimal noise reduction is achieved by optimizing the ramps of the gradient currents. Combined with other noise reduction techniques, this should lead to quieter MR scanner sequences.

A human ear is sensitive to frequencies from approximately 20 Hz to 20 kHz (32). A few studies, however, like (20, 29), show EPI noise spectra up to 10 kHz which contain relevant components above 3 kHz. Our study is the first to employ an MRI 3T system calibration (transfer function estimation) using pulses up to 4 kHz and the first to show the EPI sound pressure spectrum above this frequency range. It is also the first study to approximate gradient coil impulse responses (by superposition of third order linear systems) in order to characterize the MRI linear time invariant electro-acoustical system.

Many studies express the concern that acoustic noise during fMRI affects studies involving auditory stimuli. However, it is also possible that brain activity is always affected when using fMRI because of a reduction in the subject's attentiveness of the task (53) which leads to a reduction of brain activity (54). There is reason to assume that the brain is not a simple linear signal processor. Hence, the effects are not simply cancelled by equal exposure to stimulus and reference. Therefore, MRI acoustic noise can affect the results of any fMRI study of subject performance, not just auditory studies (29). The acoustic noise is also responsible for increasing motion artifacts that reduce detectability of brain activity (6). Quieter MRI scanners offer new possibilities to assess MRI acoustic noise effects in the results of fMRI studies of subject performance or response to any stimulus.

V. CONCLUSION

The linear time invariant electro-acoustical system approach for our 3T MRI scanner enables appropriate transfer function estimation for each gradient coil. This was demonstrated through reconstruction of the impulse responses from direct measurements of the acoustic responses to sufficiently short current pulses. We used two input specifications: (1) a theoretical gradient waveform calculated by the scanner software, and (2) an experimental recording of the gradient current. The calculated transfer functions for both input specifications are shown to be almost identical up to 4 kHz. It is noted that the step of measuring and recording gradient coils requires availability of recording tools and involves time for the calibration. Thus, the first method is encouraged when a fast and 'standard' gradient coil system characterization is desirable, and when direct measurements of gradient currents are not possible.

When analyzing the measured resonances to short pulses we noted that similar resonance modes were excited in the X and Y gradient coils (based on the four main peaks). Such modes arise either as mechanical vibration modes of the cylinder, or as acoustic resonances in the cylinder space acting as a reverberation chamber. It is known that the size and shape of the X and Y gradient coils are similar to each other; and they're both different than the Z coil (see figure 5 chapter I). Therefore, this result was not unexpected.

The electro-acoustical system (per gradient coil) for this scanner can be approximated by a superposition of third order linear systems with impulse responses: $\alpha_i t e^{-t/\tau} \Sigma_i \sin(2\pi f_i t)$ for the major spectral peaks. The time constant τ was found to be approximately 1/100 s, independent of the coil direction, which implies that its reciprocal value the damping factor is estimated to be in the 100 s^{-1} range.

The Fourier transforms of the impulse responses provide the complex (or amplitude and phase) transfer functions. These allow the computation of the acoustic response to any given pulse sequence. This is demonstrated for a specific EPI sequence. Currently, the method can predict the shape and overall spectral energy content of the measured EPI sequence signal within 2 dB. EPI waveform

prediction is an added value of this approach, and its further improvements can be applied in MRI acoustic noise control techniques.

For the analyzed 3T scanner we find that the measured echo planar imaging amplitude spectrum can be interpreted as a superposition of harmonic, non harmonic and broad band components. The acquisition time per slice (approximately 53 ms) also appears in the acoustic generated EPI waveform. It is reflected in the predicted and measured EPI spectra as constant distance (19 Hz approximately) between frequency peaks. High amplitude EPI noise is very common above 3 kHz but not often reported or discussed in the literature. However, this analysis is relevant because the normal human auditory sensitivity has a maximum at about 3 kHz and extends up to 20 kHz. It has been shown for the examined MR scanner that the acoustic response of the gradient coil system is proportional to the time derivative of the input gradient current. This interpretation supports the results by Hennel et al. (49, 50) which suggest that optimal noise reduction is achieved by optimizing the ramps of the gradient currents; and if combined with other noise reduction techniques should lead to quieter MR scanner sequences. Some studies have shown that acoustic noise during few fMRI studies affects brain activation. It is, however, not clear to which extent MRI acoustic noise affects the results in all fMRI studies of subject performance. This warrants further study of the subjective consequences, in parallel with the development of quieter MR scanners.

ACKNOWLEDGMENT

The authors would like to thank Dr. Gerke J. Hoiting for programming the signal acquisition system (scanner gradient current monitor and microphone) for the digital acquisition board (NI 6052E) employed in this study, using LABVIEW 6.0 software (NI 2000).

REFERENCES

1. Ogawa S, Lee TM, Kay AR, Tank DW. Brain magnetic resonance imaging with contrast dependent on blood oxygenation. Proc Natl Acad Sci U S A 1990;87(24):9868-9872.

2. Mc Robbie DW. MRI from picture to proton. Cambridge, United Kingdom: University Press, 2003.

3. Brummett RE, Talbot JM, Charuhas P. Potential hearing loss resulting from MR imaging. Radiology 1988;169(2):539-540.

4. Bandettini PA, Jesmanowicz A, Van Kylen J, Birn RM, Hyde JS. Functional MRI of brain activation induced by scanner acoustic noise. Magn Reson Med 1998;39(3):410-416.

5. Cho Z, Chung S, Lim D, Wong E. Effects of the acoustic noise of the gradient systems on fMRI : A study on auditory, motor and visual cortices. 39 ed. 1998. 331-335.

6. Elliott MR, Bowtell RW, Morris PG. The effect of scanner sound in visual, motor, and auditory functional MRI. Magn Reson Med 1999;41(6):1230-1235.

7. Mazard A, Mazoyer B, Etard O, Tzourio-Mazoyer N, Kosslyn SM, Mellet E. Impact of fMRI acoustic noise on the functional anatomy of visual mental imagery. J Cogn Neurosci 2002;14(2):172-186.

8. Edmister WB, Talavage TM, Ledden PJ, Weisskoff RM. Improved auditory cortex imaging using clustered volume acquisitions. Hum Brain Mapp 1999;7(2):89-97.

9. Hall DA, Haggard MP, Akeroyd MA, Palmer AR, Summerfield AQ, Elliott MR, Gurney EM, Bowtell RW. "Sparse" temporal sampling in auditory fMRI. Hum Brain Mapp 1999;7(3):213-223.

10. Melcher JR. Functional MRI of the auditory system, in medical radiology, Diagnostic Imaging and Radiation Oncology: Functional MRI, Berlin, Germany: Edited by C. Moonen and P. Bandettini (Springer), 1999. pp. 393-406.

11. Savoy R. The Psychophysical laboratory in the magnet: Stimulus delivery , Response recording, and safety, in medical radiology, Diagnostic Imaging and radiation oncology: Functional MRI. Berlin: Springer, edited by C. Moonen and P. Bandettini , pp. 347-365. 1999..

12. Ravicz ME. Reducing imager generated noise at the ear during functional magnetic resonance imaging: Passive attenuation, Abstracts of the twenty first midwinter meeting of the association for research in otolaryngology (ARO, Mt. Royal, NJ), p. 208. 1998.

13. Ravicz ME. Imager noise and noise reduction during fMRI, Neuroimage 7 (4) , S556. 1998b.

14. Mansfield P, Glover PM, Beaumont J. Sound generation in gradient coil structures for MRI. Magn Reson Med 1998;39(4):539-550.

15. Hedeen RA, Edelstein WA. Characterization and prediction of gradient acoustic noise in MR imagers. Magn Reson Med 1997;37(1):7-10.

16. Barnett A. Comments on "gradient-induced acoustic and magnetic field fluctuations in a 4T whole-body MR imager". Magn Reson Med 2001;46(2):207.

17. Hoiting GJ. "Measuring MRI noise". PhD Thesis, 2005. ISBN 90-367-2235-7 (Online version).

18. More SR, Lim TC, Li M, Holland CK, Boyce SE, Lee JH. Acoustic noise characteristics of a 4 Telsa MRI scanner. J Magn Reson Imaging 2006;23(3):388-397.

19. McClellan JH, Schafer RW, Yoder, M. A. Signal Processing First. Pearson Prentice Hall. 2003. International edition. Chapters 5, 6 and 10.

20. Counter SA, Olofsson A, Grahn HF, Borg E. MRI acoustic noise: sound pressure and frequency analysis. J Magn Reson Imaging 1997;7(3):606-611.

21. Shellock FG, Morisoli SM, Ziarati M. Measurement of acoustic noise during MR imaging: evaluation of six "worst-case" pulse sequences. Radiology 1994;191(1):91-93.

22. Mcjury MJ. Acoustic noise levels during magnetic resonance imaging scanning at 1.5 T. Br. J. radiol. 67, 413-415, 1994.

23. McJury MJ. Acoustic noise levels generated during high field MR imaging. Clin Radiol 1995;50(5):331-334.

24. Hurwitz R, Lane SR, Bell RA, Brant-Zawadzki MN. Acoustic analysis of gradient-coil noise in MR imaging. Radiology 1989;173(2):545-548.

25. Miyati T, Banno T, Fujita H, Mase M, Narita H, Imazawa M, Ohba S. Acoustic noise analysis in echo planar imaging: multicenter trial and comparison with other pulse sequences. IEEE Trans Med Imaging 1999;18(8):733-736.

26. Cho ZH, Park SH, Kim JH, Chung SC, Chung ST, Chung JY, Moon CW, Yi JH, Sin CH, Wong EK. Analysis of acoustic noise in MRI. Magn Reson Imaging 1997;15(7):815-822.

27. Wessinger CM. Tonotopy in human auditory cortex examined with functional magnetic resonance imaging. Human Brain mapp. 5, 78-25, 1997.

28. Counter SA, Olofsson A, Borg E, Bjelke B, Haggstrom A, Grahn HF. Analysis of magnetic resonance imaging acoustic noise generated by a 4.7 T experimental system. Acta Otolaryngol 2000;120(6):739-743.

29. Ravicz ME, Melcher JR, Kiang NY. Acoustic noise during functional magnetic resonance imaging. J Acoust Soc Am 2000;108(4):1683-1696.

30. Cohen M. Theory of echo-planar imaging., in Echo-Planar Imaging: Theory, technique and application, edited by F. Schmitt, M. K. Stehling, and R. Turner (Springer, Berlin), pp. 11-30. 1998.

31. Prieto TE. Acoustic noise levels in a head gradient coil during echo planar imaging. Proceedings of the international society for magnetic resonance in medicine, sixth scientific meeting and exhibition. P. 750. 1998.

32. Kinsler LE. Fundamentals of acoustics. John Wiley and Sons, Inc. 2000.

33. Randall RB. Frequency Analysis. Third edition. Bruel & Kjaer. 1987.

34. Gazdzinski C, Mechefske CK. Acoustic noise measurements in a 4T Whole-Body MRI scanner. Proc. Intl. Soc. Mag. Reson. Med. 10 (2002).

35. Kay SM. Modern Spectral Estimation.Englewood Cliffs, NJ: Prentince Hall, 1988. Pg. 454. 2007.

36. Hayes MH. Schaum's outline of theory and problems of digital signal processing. Mc-Graw Hill companies Inc. 1999. Chapter 9, p 361.

37. Beranek LL. Acoustical Measurements. Acoustical Society of America 1988. Chapter 20.

38. Tomasi DG, Ernst T. Echo planar imaging at 4 Tesla with minimum acoustic noise. Journal of Magnetic Resonance Imaging 2003;18(1):128-130.

39. Tomasi D, Ernst T. A simple theory for vibration of MRI gradient coils. Brazilian Journal of Physics, vol. 36, no. 1A, March, 2006.

40. Li W, Mechefske CK. Acoustic Noise Analysis and Prediction in a 4-T MRI scanner" Concepts in Magnetic Resonance Part B (Magnetic Resonance Engineering) Vol. 21B(1): 19-25, 2004.

41. Edelstein WA, Hedeen RA, Mallozzi RP, El Hamamsy SA, Ackermann RA, Havens TJ. Making MRI quieter. Magn Reson Imaging 2002;20(2):155-163.

42. Katsunuma A, Takamori H, Sakakura Y, Hamamura Y, Ogo Y, Katayama R. Quiet MRI with novel acoustic noise reduction. MAGMA 2002;13(3):139-144.

43. Chambers J, Akeroyd MA, Summerfield AQ, Palmer AR. Active control of the volume acquisition noise in functional magnetic resonance imaging: method and psychoacoustical evaluation. J Acoust Soc Am 2001;110(6):3041-3054.

44. Chen CK, Chiueh TD, Chen JH. Active cancellation system of acoustic noise in MR imaging. IEEE Trans Biomed Eng 1999;46(2):186-191.

45. Elliot SJ, Nelson P. Active noise control. IEEE Sign. Proc. Magn. 12-35, 1983.

46. Goldman AM, Gossman WE, Friedlander PC. Reduction of sound levels with antinoise in MR imaging. Radiology 1989;173(2):549-550.

47. McJury M, Stewart RW, Crawford D, Toma E. The use of active noise control (ANC) to reduce acoustic noise generated during MRI scanning: some initial results. Magn Reson Imaging 1997;15(3):319-322.

48. McJury M, Shellock FG. Auditory noise associated with MR procedures: a review. J Magn Reson Imaging 2000;12(1):37-45.

49. Hennel F, Girard F, Loenneker T. "Silent" MRI with soft gradient pulses. Magn Reson Med 1999;42(1):6-10.

50. Hennel F. Fast spin echo and fast gradient echo MRI with low acoustic noise. J Magn Reson Imaging 2001;13(6):960-966.

51. Loenneker T, Hennel F, Ludwig U, Hennig J. Silent BOLD imaging. MAGMA 2001;13(2):76-81.

52. Marcar VL, Girard F, Rinkel Y, Schneider JF, Martin E. Inaudible functional MRI using a truly mute gradient echo sequence. Neuroradiology 2002;44(11):893-899.

53. Paschler HE. The psychology of attention (MIT Press, Cambridge, MA). 1998. 494 pp.

54. Woodruff PW, Benson RR, Bandettini PA, Kwong KK, Howard RJ, Talavage T, Belliveau J, Rosen BR. Modulation of auditory and visual cortex by selective attention is modality-dependent. Neuroreport 1996;7(12):1909-1913.

CHAPTER III.

MRI ACOUSTIC NOISE REDUCTION BY DESTRUCTIVE INTERFERENCE OF RESONANCE FREQUENCIES[1]

Marcel Segbers, Carlos V. Rizzo S, Hendrikus Duifhuis and Johannes M. Hoogduin

—A method to reduce the acoustic noise generated by gradient systems in magnetic resonance imaging (MRI) is proposed based on the linear response theory: destructive interference of resonance frequencies. Since the physical cause of MRI acoustic noise is the time derivative of the gradient current, a common trapezoid current shape only excites the gradient in the rising and falling edge. In the falling edge the coil is excited with 180 degree phase difference with respect to rising edge. Therefore, by varying the width of the trapezoid and keeping the ramps constant, it is possible to suppress one selected frequency and its higher harmonics. This value is matched to one of the prominent resonance frequency of the gradient coil system. The idea of cancelling a single frequency is extended to a second frequency using two successive trapezoid shape pulses presented at a selected interval. Sound pressure level (SPL) reduction of 6 and 10 dB is found for the two trapezoid shapes and a single pulse shape, respectively. The proposed pulse shapes are additionally tested in a simulated echo planar imaging (EPI) read out train obtaining SPL reduction of 12 dB for the best case.
Index Terms—acoustic noise reduction, fMRI, gradient noise, linear system, silent imaging, SPL.

[1] Portions of this material were presented as traditional poster (1349) at the 16th scientific meeting and exhibition of the international society for magnetic resonance in medicine, Toronto, Canada, 6 May 2008. In addition, a modified version of this manuscript is (in preparation) to be submitted for publication.

I. INTRODUCTION

Magnetic Resonance Imaging (MRI) allows mapping of body structure and function used for both clinical and basic research. However, the acoustic noise produced by MRI scanners is a major concern because it reaches safety limits in many cases (1), specially, during the so-called rapid sequences (1-4). The sources of this noise are the pulses of current supplied to the gradient coil for the spatial encoding of the NMR signal. The frequency spectrum of the scanner noise is equal to the product of the input gradient current function and the electro-acoustical transfer function of the gradient system (5). This acoustic noise causes additional discomfort and anxiety in patients (6) and represents an obstacle in functional MRI studies of the auditory cortex (7, 8). Increasing the static magnetic field and field gradients for clinical and research MRI applications makes the problem of acoustic noise more critical. In addition to the use of sound-attenuating materials, many methods of MRI acoustic noise reduction have been proposed such as active noise cancellation (9), destructive sound interference in gradient coil design (10), and sound attenuation by vacuum layers (11).

Recently it has been suggested that the acoustic response of the MR gradient coil system is proportional to the time derivative of the input gradient current (12). Therefore, decreasing the slew rate whilst increasing rise time results in lowering sound pressure level, supporting the results reported in silent imaging (13, 14). However, the drawback of this technique is the increase in scan time and its effect on image quality. We introduce a pulse shape consisting of two trapezoids designed to reduce the acoustic noise levels while minimizing to some extent scan time. This pulse shape optimization is in agreement with the proposed vibrating string model approximation for MRI acoustic noise suppression (15-17). The acoustic noise reduction is achieved by timing the ramps of the trapezoids such that two resonance frequencies of the MR scanner gradient coil transfer function are eliminated. Zeros in the gradient current spectrum can be set to selected frequencies, such as the two most prominent resonance frequencies in the gradient coil transfer function. Therefore, our work is aimed at:

1. showing, by means of a comprehensive Lorentz force model of the displacement of a point in a gradient coil, the relation between the time derivative of the gradient input currents and the generated MRI sound (see appendix);
2. showing experimentally the MRI electro-acoustical relation by using pulses with different lengths and by estimating the transfer function based on these different inputs;
3. measuring and predicting the acoustic noise generated by two optimized pulses and compare them with noise measurements generated by sinusoidal shape and triangular pulses, common in silent imaging.

Finally, the proposed pulse shapes are tested in a simulated echo planar imaging (EPI) read out train. By using appropriate timing of the ramps of the trapezoids again, one resonance frequency is eliminated and the fundamental frequency (inverse of pulse train period) is placed in a dip of the transfer function.

II. THEORY

A single trapezoid shape current[2] (figure 1a) with duration time t_T full width half maximum FWHM, (at 50% height) much greater than rise and fall times t_R excites the gradient coil acoustically in the rising and falling edges. On the falling edge the coil is excited with 180 degree phase difference with respect to the rising edge. By varying t_T whilst keeping the t_R s constant, it is possible to eliminate one specific frequency and its higher harmonics. That is, at the frequency $f_1 = 1/t_T$ the interference at the falling edge is destructive, cancelling generated noise for this frequency (figure 1a). Note that similar suppression occurs at $1/t_R$, but, obviously if $t_T >> t_R$ that frequency is much higher than $1/t_T$, and usually is beyond the range of primary interest. All this follows directly from the fact that a given trapezoid can be considered the convolution of two rectangular blocks of durations t_T and t_R (figure 1b). The spectra of which are sinc-

[2] Most of the pulse sequences used in MRI consists of trapezoid pulse shapes.

functions[3] with the first zeros at 1/*t*, where *t* represents the block durations. In other words, the spectrum of the trapezoid is the product of the two sinc-functions. Therefore, a slightly longer trapezoid shape with $t_T > t_R$ is suitable for selective frequency ($1/t_R$) suppression.

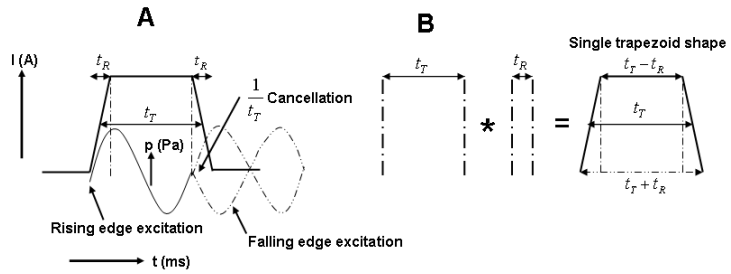

FIG. 1. A) Destructive interference of a single frequency on the second ramp. B) Trapezoid as the convolution of two blocks.

The idea can be extended to a second frequency by using two trapezoid shape current pulse of opposite sign (figure 2a). Such a signal can be considered the convolution of a single trapezoid t_T at FWHM and the signal, $\delta(t) - \delta(t - t_T - t_2)$ in other words, with two delta-functions (figure 2a). These two are equivalent to the time-derivative of a (unit) block of duration $(t_T + t_2)$ and hence, the spectral representation will be $j\omega$ times[4] the sinc-spectrum with its first zero at $f_2 = \frac{1}{t_T + t_2}$ hence, f_2 will now also be eliminated. Pulse train current shapes are more useful for MRI imaging than isolated pulse shapes. Such a train is a very simple model of an EPI read out train. The amplitude of the trapezoids determines the speed at which a line in k-space is acquired. The acquisition time is thus determined by

---

[3] $\text{sinc}(x) = \frac{\sin(x)}{x}$.

[4] A function and its time derivative are related in the Fourier domain by $F\{\frac{\partial}{\partial t} h(t)\} = j\omega H(\omega)$.

the maximum amplitude and by how fast the gradients can change (slew rates), see figure 2.

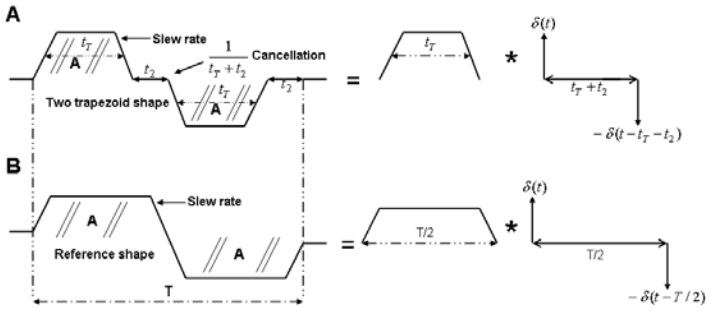

FIG. 2. A) Destructive interference for two frequencies. Creation of two trapezoid shape by convolution with delta functions. B) Reference shape.

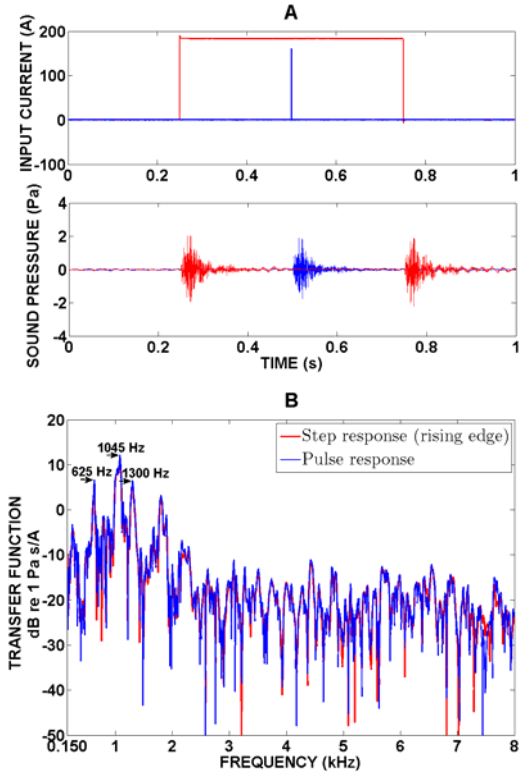

FIG. 3. A) Input train of pulses and output acoustic response. B) Transfer function (X-gradient coil) based on rising step input (adjusted) and based on pulse input.

Pulse shapes which have equal area cover the same line in k-space, albeit at different speeds. Therefore, to make a proper comparison in terms of produced sound between pulse shapes, the area of the pulse is kept constant (figure 2b). The trapezoid is the time optimum pulse shape since both slew rate and amplitude are maximal. Other pulse shapes designed for acoustic noise reduction increase scan time. The measured input currents (for pulse in blue and step inputs in red) and output sound pressures (blue and red, respectively) are shown in figure 3a; the step input current can be divided into two input specifications, one for the rising and one for the falling edge. Assuming the input gradient current to be completely symmetric, the time derivative of the rising and falling edge differ only by sign (or 180 degrees phase difference). Since MRI transfer function deals with input current signals, it implies this transfer function can be obtained for any of these two input specifications (the rising or the falling edge). Since a function and its time derivative are related in the Fourier domain, the transfer function using rising edge as input is related by the factor $j\omega$ to one estimated using the pulse response. The appendix shows for a more comprehensive Lorentz force model the relation between gradient input time derivative currents and MRI produced sound.

III. METHODS

The experiment was performed on a Philips Intera 3 Tesla MR scanner [maximum gradient strength 21 milliTesla(mT)/meter(m) per axis], located at the Behavioral and Cognitive Neurosciences (BCN) NeuroImaging Center (NiC) at the University of Groningen, The Netherlands. We employed a non-magnetic microphone support specially fitted to the edges of the patient's table inside the imager bore. To record sound inside the scanner (isocenter) a 1/2 inch condenser microphone Bruel Kjaer (B&K) 4190 (tested for MRI in (18)) was mounted on this support and connected to a preamplifier (B&K ZC0026). Before measurements microphone and preamplifier were calibrated using sound level calibrator 4230 [B&K, $\approx$ 94 dB at 1000 Hertz (Hz)]. This microphone and preamplifier are connected to a B&K Modular Precision Sound Analyzer 2260 through a 10 meter long extension cable (B&K AO0442). The 3T scanner used in this study supports a maximum current amplitude of approximately 700 Amperes (A), which can be read out using a manufacturer provided

current monitor signal of 10 Volts (V), that is, 10V ≅ 700A, for each gradient coil. Acquisition of the scanner gradient current monitor signal and of the microphone signal takes place via a 16 bits digital acquisition board (National Instruments 6052E) using LABVIEW 6.0 software (National Instruments 2000). Since no radio frequency (RF) signals are used for these measurements, a phantom was not needed, and the receiver RF head coil was removed from the scanner. All analog signals are low-pass filtered (Kemo Inc., 8-pole Bessel, cut-off frequency 14 kHz) before acquisition and are sampled at 100 kHz. The data were analyzed using the MATLAB signal analysis toolbox (R2006a). Two input sequences were recorded with the generated output sound in addition to background noise levels, whilst the helium coolant pump for the imager's permanent magnet was turned off. First the pulse response: 25 calibration trapezoidal pulses [0.1 milliseconds (ms) raise and fall times, 0.01 ms plateau time, 10 mT/m amplitude] were presented to the X-gradient coil at 0.5 seconds (s) intervals. This procedure was repeated for Y and Z gradients. The second sequence was used for the step response: 25 calibration trapezoidal pulses [0.1 milliseconds (ms) raise and fall times, 250 ms plateau time, 10 mT/m amplitude] were presented to the X-gradient coil at 0.5 seconds (s) intervals. This procedure was repeated for Y and Z gradients.

Trapezoid shape

To test the properties of a single trapezoid pulse with $t_T >> t_R$, the sound pressure level (SPL) produced using constant amplitude 10 mT/m and slew rate 100 mT/m/ms is recorded and compared. Since the amplitude is constant, the total area varies as function of the average duration (t_T), which is varied between 0.11 ms and 2.9 ms in 13 steps. In a second experiment the total area and slew rate are kept constant at 10 mTms/m and 110 mT/m/ms respectively, whereas, t_T varied between 0.5 ms and 3 ms in steps of 0.1 ms. Since area is constant, amplitude varies as function of the average duration. In a third experiment the SPL of this pulse shape is compared with sinusoidal (special and round cosine) and triangle shapes. For a correct comparison between all pulse shapes, the area under the pulse as well as the time duration are kept constant. The generated acoustic noise is measured for all pulse shapes. The total duration of the pulse shapes varies between 0.75 ms and 2.5 ms, total area is kept constant at 10 mTms/m. The triangle has the minimum slew rate for the given

duration and area. The cosine pulse is a simple cosine between $-\pi/2$ and $\pi/2$. Another sinusoidal pulse is made by adding one to a cosine function between $-\pi$ and π, making a cosine square which has smooth edges in the time domain. In order to create and employ user defined pulse shapes on the MRI scanner a patch with small modifications was written in the pulse programming software environment. The sampled pulse shapes must have a sampling frequency of 156.25 kHz; and a maximum of 150000 samples can be supplied. The maximum length of user defined pulse duration was 96 ms. The following sampled pulse shapes were constructed in MATLAB and written to a text file: two trapezoid shapes, cosine shape, cosine square and triangle shape. Another (longer) single trapezoid pulse with $t_T > t_R$ that is, t_T = 1.6 ms and t_R = 0.96 ms is created; its generated acoustic noise compared with two references, a trapezoid (maximum slew rates) and a triangle (minimum slew rates) with an equal area of 20 mTms/m and the same duration.

Two trapezoid shape

The two trapezoid pulse is designed with t_T = 0.96 ms, which matches the first resonance frequency and t_2 is varied between 0 ms and 2.5 ms in steps of 0.1 ms. Each of the two trapezoids (see figures 2A and 2B) covers an area of 10 mTms/m and slew rates are kept constant at 110 mT/m/ms. A shorter pulse shape with t_T = 0.8 ms and t_2 = 0.19 ms is also designed. For the EPI like sequence, the two trapezoid pulse is repeated 19 times with t_T = 1 ms and t_2 = 0.5 ms. Its generated acoustic noise is compared in a similar pulse train manner (constant duration and area) with reference cosine, trapezoid and triangle shapes. Creating EPI like read out train based on repetition of a two trapezoid shape with period T (figure 2b) is achieved with the following specifications: the duration of a (single) two trapezoid shape is chosen in order to match the fundamental frequency f_c (1/T) to a minimum of the transfer function. In terms of t_T and t_2: $f_c = \frac{1}{2(t_T + t_2)}$; whereas t_T is chosen such that it cancels the main resonance peak frequency from the transfer function; and t_2 is chosen such that the fundamental frequency matches a minimum of the transfer function. To estimate the effect of the fundamental frequency, a pulse train of trapezoids with a fundamental frequency equal to the

main resonance frequency (1045 Hz, see figure 3B) is used to excite the gradient coils maximally. To reduce the sound pressure level a fundamental frequency that matches a minimum of the transfer function (921 Hz, based on measurements of the transfer function in Figure 3B) is employed. The area of these trapezoids are kept constant at 10 mTms/m. Cancelling the main resonance frequency whereas the train fundamental frequency matches a minimum of the transfer function is further investigated by using a two trapezoid pulse with t_T = 1 ms and t_2 = 0.45 ms, ensuring a fundamental frequency of approximately 350 Hz.

IV. RESULTS AND DISCUSSION

Trapezoid shape

Generated noise during calibration process (figure 3a) was 84, 76 and 76 dB (SPL) for X, Y and Z gradient coils respectively. Background noise was 67 dB (SPL), due to ventilating and cooling system. A comparison between the rising edge (multiplied by the appropriate factor) input based transfer function (red) and one estimated by pulse response input (blue) shows good agreement for the X gradient coil (figure 3b). Transfer function main resonance frequencies for all coils are shown in table I. Measured and predicted sound pressure levels as a function of duration for trapezoids with equal amplitude are plotted in figure 4a. In the measured sound spectrum of trapezoid of 0.92 ms duration (not shown) the resonance frequency of 1045 Hz is eliminated completely; this represents the minimum in figure 4a. When the areas of the trapezoids are kept constant and the pulse shape duration varies, the minima in measured sound spectrum are at t_T = 1 ms and 1.7 ms. That is, the minima in figure 4a are reduced to plateaus. Keeping the area constant makes the pulse amplitude decrease proportionally to the duration of the pulse, resulting in lower sound pressure level and flattening of the minima. An overview of the created pulse shapes is depicted in figure 4b, in this case the pulses last 2 ms each and the areas are constant at 10 mTms/m. Sound pressure levels for the trapezoid, triangle, cosine, and cosine square are shown in figure 4c. For very short pulses the trapezoid produces less noise than other shapes.

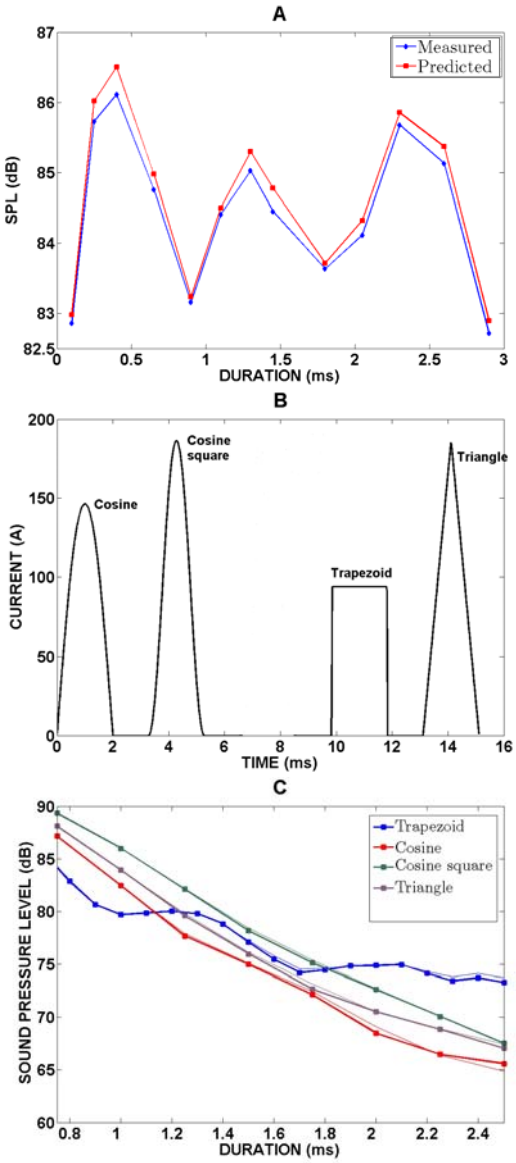

FIG. 4. A) Measured and predicted sound pressure level for single trapezoids, equal amplitude as function of t_T . B) Different pulse shapes employed. C) Sound pressure levels of different pulse shapes. Thick and thin line: Recorded and predicted value.

For these short pulses the amplitude is probably the most important factor which is almost two times higher for the other shapes than the

trapezoid (figure 4b). The slew rates for these durations (for all shapes) are near the maximum value allowed in the scanner and do not differ markedly. At approximately 1.2 ms the cosine is more silent than the trapezoid. The amplitude of the frequencies higher than the inverse of the full width half maximum (FWHM) is much lower for the cosine pulse, and therefore suppresses the main resonance peak better then the trapezoid. After 1.7 ms the noise of the trapezoid remains constant, noise is produced on the ramps, slew rate does not change, only the amplitude drops slightly. Eventually, all pulse shapes become more silent than the trapezoid, because the slew rates of these pulses decrease with the duration, whereas trapezoid slew rate remains constant. The cosine square produces more noise than the cosine because it has slightly higher slew rates. Measured and predicted sound pressure level for the longer trapezoid (t_T = 1.6 ms, t_R = 0.96 ms) pulse and the references are shown in table II. Predictions accurately match the experimental measurements. The amplitude spectrum of this pulse is shown in figure 5a. As expected, its input amplitude spectrum contains minima at the first three main resonance peaks (625 Hz, 1045 Hz, and 1300 Hz) since the third peak is near the second harmonic of 625 Hz. This longer pulse designed as the convolution of two blocks of comparable lengths is 10 dB more silent than reference trapezoids and 3 dB more silent than triangular pulse references. However, since the length of this single pulse is longer compared to already mentioned single trapezoid shapes, its use in EPI read our train was not investigated.

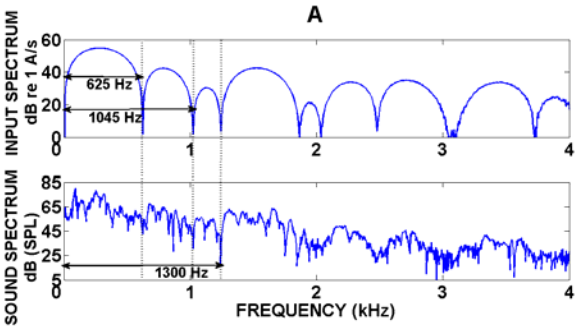

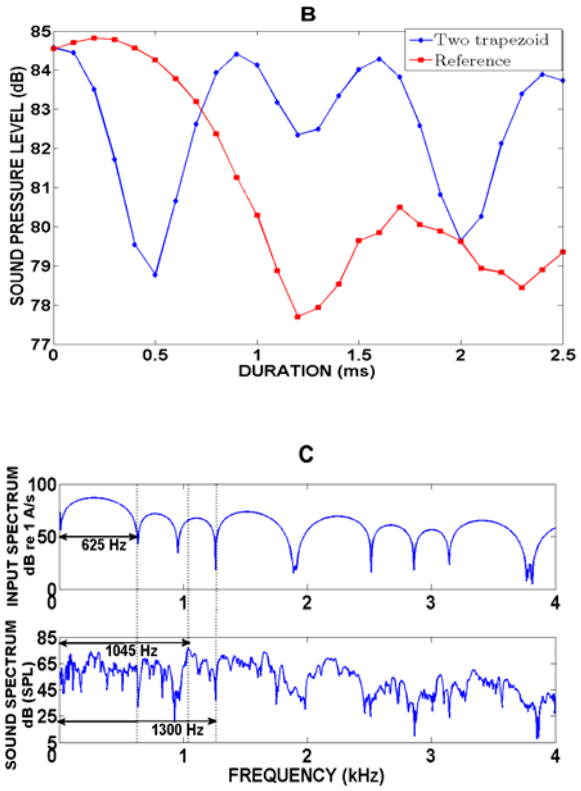

FIG. 5. A) Top and bottom: Input amplitude spectrum and pressure spectrum for longer trapezoid pulse (t_T = 1.6 ms, t_R = 0.96 ms) respectively. B) Measured sound pressure level for the two trapezoid pulse (as a function of t_2 , t_T is constant 0.96 ms) and the reference. C) Top and bottom: Input amplitude spectrum and pressure spectrum of two trapezoid pulse shape respectively.

Two trapezoid shape

Sound pressure levels for the two trapezoid shapes as function of t_2 (t_T is fixed at 0.96 ms) are shown in figure 5b. Maximum difference with reference pulse of approximately 6 dB is realized for t_2 = 0.5 ms. For larger values of t_2, the two trapezoid shape is noisier than the reference since the amplitude of the reference decreases with the parameter t_2, whereas the amplitude of the two trapezoid shape

remains constant. The reference pulse has a minimum in sound pressure level around 1.2 ms duration. This is approximately 0.2 ms higher than the value found for the single trapezoid. In this experiment however, longer pulse shapes have lower amplitude, reducing the sound pressure level even more. This should explain the observed difference. The sound pressure level prediction from the sampled input is slightly higher than the measured sound pressure levels. This happens because the actual pulse sent to the scanner is slightly deformed due to eddy current compensation; therefore, there is a small difference between the programmed and the actual pulse. The input amplitude spectrum of the optimal two trapezoid shape (t_2 = 0.5 ms) is shown in figure 5c. It is expected to contain three minima around 684 Hz ($\frac{1}{t_T + t_2}$), 1041 Hz ($\frac{1}{t_T}$) and 1368 Hz (first minimum second harmonic). However, the measured minima values are slightly different: 628 Hz, 960 Hz and 1262 Hz. These values approximate the main resonance peaks 625 Hz, (to less extent) 1045 Hz, and 1300 Hz. Therefore, a reduction of the first and third resonance frequencies is observed in the sound spectrum; a reduction of the second resonance frequency is achieved to a lesser extent. The sound spectrum of the reference pulse still contains the resonance peaks of the transfer function; therefore it produces a higher sound pressure level.

Frequency (Hz)	**X-Gradient Peak Height (dB)**	**Frequency (Hz)**	**Y-Gradient Peak Height (dB)**	**Frequency (Hz)**	**Z-Gradient Peak Height (dB)**
625	8	645	6	1180	0
1045	13	1030	3	1345	7
1300	10	1395	1	1580	3

TABLE I. Frequency and height of main resonance peaks for all gradient coils.

Pulse shape	**Measured SPL (dB)**	**Predicted SPL (dB)**
Longer Trapezoid	76	76
Trapezoid	86	86
Triangle	79	79

TABLE II. Sound pressure levels for the longer pulse (t_T = 1.6 ms, t_R = 0.96 ms) and the reference.

Fundamental frequency (Hz)	Trapezoid SPL (dB)	Cosine SPL (dB)	Triangle SPL (dB)	Two trapezoid shape SPL (dB)
1045	108 (114)	109 (115)	108 (115)	-
921	96 (97)	97 (98)	96 (99)	-
310	88 (87)	-	85 (83)	89 (88)
390	-	-	92 (91)	97 (98)
350	100 (102)	-	94 (95)	88 (87)

TABLE III. Measured and predicted (brackets) sound pressure levels of different pulse trains.

Table III summarizes the measured and predicted sound pressure levels for different pulse shapes in a pulse train. The fundamental frequency of the first pulse train matches the coil resonance frequency of 1045 Hz. The second train has a fundamental frequency (921 Hz) equal to a minimum in the transfer function but near the resonance frequency (1045 Hz). The two trapezoid shape train which cancel the resonance frequency of 625 Hz and 1045 Hz has a fundamental frequency of 310 Hz. The two trapezoid shape cancelling the resonance frequencies of 1045 Hz and 1300 Hz has a fundamental frequency of 390 Hz. Finally, another two trapezoid shape fundamental frequency matching a minimum in the transfer function (350 Hz) is presented.

The sound pressure level produced by the pulse train with the fundamental frequency matching a minimum of the transfer function (921 Hz) is approximately 12 dB lower than a pulse train with the fundamental frequency matching the maximum of the transfer function (1045 Hz). No effect of the shape of the pulse is observed. For the pulse train which fundamental frequency matches the higher resonance frequency, the predicted values are approximately 6 dB higher than the measured values. This might indicate that for this extreme case, exciting the gradient coil maximal at the main resonance frequency, the system might not behave completely linear. The optimal two trapezoid shape train with fundamental frequencies 310 Hz and 390 Hz does not reduce the output noise. It seems as loud as a pulse train consisting of simple trapezoids and is 4 dB louder than the triangle pulse train. The amplitude spectrum for this case is shown in figure 6a. The graph shows a maximum for both the triangle and the

two trapezoid shape at the fundamental frequency. The two trapezoid shapes have no maxima near the main resonance frequencies as expected. The triangle shows a distinct minimum between 1100 Hz – 1400 Hz, which possibly explains the 4 dB noise reduction for the triangle. The two trapezoid shape at 390 Hz show similar difference (5 dB) with the triangle. Their amplitude spectra in figure 6b presents a minimum between 1300 Hz – 1600 Hz present in the triangle and two trapezoid shape.

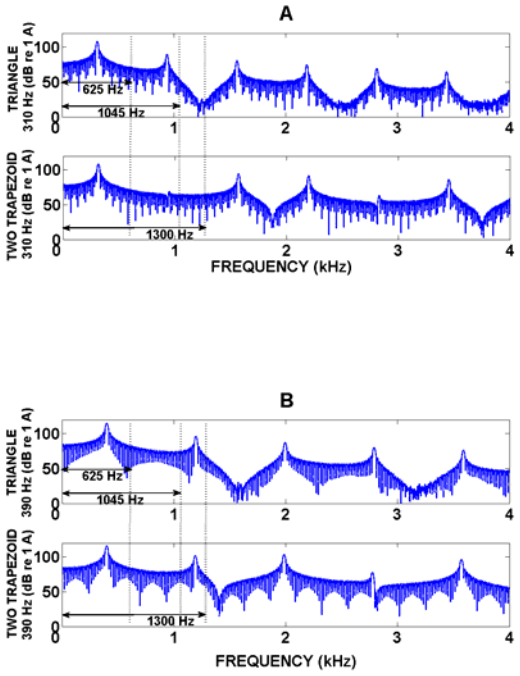

FIG. 6. A) Top and bottom: Input amplitude spectrum of triangle and two trapezoid pulse shape respectively with fundamental frequency 310 Hz. B) Top and bottom: Input amplitude spectrum of triangle and two trapezoid pulse shape respectively with fundamental frequency 390 Hz.

The two trapezoid shape train with the fundamental frequency matching a minimum of the transfer function at 350 Hz shows significant reduction in sound pressure level compared to the trapezoid pulse train (-12 dB) and even compared with the triangle pulse train (-6 dB). When comparing the spectra of the triangle and

the two trapezoid shape, it is seen that the spectrum of the triangle has a maximum at resonance frequency (1045 Hz) which is absent in the spectrum of the two trapezoid shape, since the latter was specifically designed to reduce this main resonance frequency.

All proposed pulse shapes and predictions are optimized for one gradient coil direction only (X). The resonance frequency values for the Y-gradient coil are similar to the X-gradient coil values, whereas, Z-gradient coil resonance frequencies differ to some extent (Table I). Therefore, these optimized pulse shapes can be easily implemented to the other gradient coils and count for total sound pressure level reduction. We propose a pulse shape optimization fixed to the MRI gradient coil resonance frequencies. If these frequencies could be increased by slight modifications of existing coils, the duration of our pulse shapes would be shorter and very suitable for fast (EPI like) sequences. In detail, since the proposed noise reduction method is based on interference of gradient coil main resonance frequency; and for optimized time pulse shapes this is inversely proportional to resonance frequency; therefore, very fast pulses 0.1 ms length for example could reduce a resonance frequency of 10 kHz. This very fast pulse shape then would be very useful if MRI resonance frequencies could be increased, however, now there is a limit in optimized pulse shape length due to the main resonance frequencies around 500 Hz – 1500 Hz. Further research adding this technique to current MRI noise reduction strategies could lead to further noise reduction gains.

V. CONCLUSION

A 3T MR electro-acoustical transfer function is determined by measuring a slightly different input specification shown to be related to the traditional one by a simple mathematical relation. This new transfer function falls of for higher frequencies as expected for a physical system. Our experiments including the first order Lorentz forces physical model have shown the correctness to treat the time derivative of the gradient current as the physical cause of the acoustic noise. The advantage of this new interpretation is exploited in pulse sequence optimization for MRI acoustic noise reduction. That is, an MRI noise reduction technique based on destructive interference of resonance frequencies is presented and proposed to reinforce the silent pulses concepts while attaining further reduction gains. For isolated pulse shapes the sound pressure spectrum can be optimized to cancel

out main resonance frequencies in the transfer function. A single trapezoid of 1ms approximate duration cancels the main resonance frequency of our facility (1045 Hz). The two trapezoid shape of 2.92 ms approximate duration reduced the three main resonance frequencies 625 Hz, (to a lesser extent) 1045 Hz and 1300 Hz. This leads to a reduction in sound pressure level (SPL) of maximum 6 dB for the two trapezoid shape with respect to a trapezoid reference. The same resonance frequencies are completely eliminated by constructing a longer trapezoid pulse (2.6 ms) achieving a reduction of 10 dB SPL relative to a trapezoid reference. For shorter durations (less than 1.5 ms), no advantage in the use of sinusoidal pulse shapes is observed in our study. For longer durations, sinusoidal pulse shapes reduce the sound pressure level relative to the trapezoid. Creating a pulse train out of the optimal two trapezoid shape does not lead to a higher reduction in sound pressure level in our MR scanner. The pulse train fundamental frequency becomes a dominant factor; a large difference in sound pressure level is observed when the pulse train fundamental frequency matches a minimum and then a maximum of the transfer function. This pulse train reduces the SPL 12 dB as compared to the trapezoid pulse train and 6 dB SPL as compared to a triangle pulse train. The approach of pulse shape optimization described here can be easily implemented in any facility (using all gradient coil directions X, Y and Z) counting on total sound pressure level reduction. If the MRI gradient coil resonance frequencies could be increased, the duration of optimized pulse shapes would be very useful for fast sequences, since the pulse duration is inversely proportional to the scanner resonance frequency (to eliminate). Additional research could explore further MRI noise reduction gains by adding this technique to current noise reduction strategies.

VI. APPENDIX

The Lorentz force linked to electrical current deforms the gradient coils and stores potential (deformation) and kinetic energy (coil vibration) in the gradient coils system (19). The surface of the gradient coils sets air molecules in motion which will be perceived as sound. This can be described as a linear time invariant (LTI) system. A simple LTI model of the displacement of a point in the gradient coil is given in equation 1, relating the displacement to the Lorentz force. Let $F(\omega)$ be the Fourier transform of the Lorentz force $f(t)$; and let

$X(\omega)$ be the Fourier transform of the displacement $x(t)$. In this first simple approximation the above mentioned quantities are related to each other by the transfer function $H(\omega)$:

$$X(\omega) = H(\omega)F(\omega); \quad (1)$$

Part of the kinetic energy is transmitted to the air as sound waves. Since the kinetic energy depends on the velocity (time derivative of displacement), the time derivative is taken both sides of equation 1 to obtain:

$$V(\omega) = j\omega H(\omega)F(\omega); (2)$$

Close to the gradient coil vibrating surface, the particle speed in air (V_{air}) is approximated to the gradient coil surface speed (V). For acoustic waves, pressure and velocity are related by the acoustic impedance z (equation *3*); however for MRI scanners the acoustic impedance is not easy to estimate given the sound field complexity. Therefore, three simple cases will be treated to obtain an approximation of the dependence of acoustic impedance and frequency for MRI scanners.

$$V_{air} = \frac{p}{z}; \quad (3)$$

For plane waves the specific impedance (20) is a product of the air density ρ_0 and the speed of sound c, that is: $z = \rho_0 c$; *(4)*

The acoustic waves inside the MRI scanner can be spherical or like the geometrical shape of the scanner, cylindrical of nature. For spherical waves the specific acoustic impedance is given by (20):

$$z = \rho_0 c \cos(\theta) e^{j\theta} ; (5)$$

θ is calculated from:

$$\cot(\theta) = kr ; (6)$$

The distance from the sound source is r and $k = \frac{w}{c}$ is the wave number. For cylindrical waves the relation is given by (20):

$$z = j\rho_0 c \frac{H_0^2(kr)}{H_1^2(kr)}; (7)$$

In equation 7, H_0^2 and H_1^2 are Hankel functions of second kind. The gradient coil have a radius of approximately 0.35 m, this means that in the isocenter the sound sources are at least at 0.35 m distance. The

relation between real and imaginary part of the specific impedance and the frequency for this distance is shown in figure 7 for all three cases discussed above. For acoustic waves with frequency 500 Hz (approximately) and higher, the impedance for both fields approach the impedance of plane waves, since imaginary part is small compared to the real part and the real part approaches the impedance of plane waves.

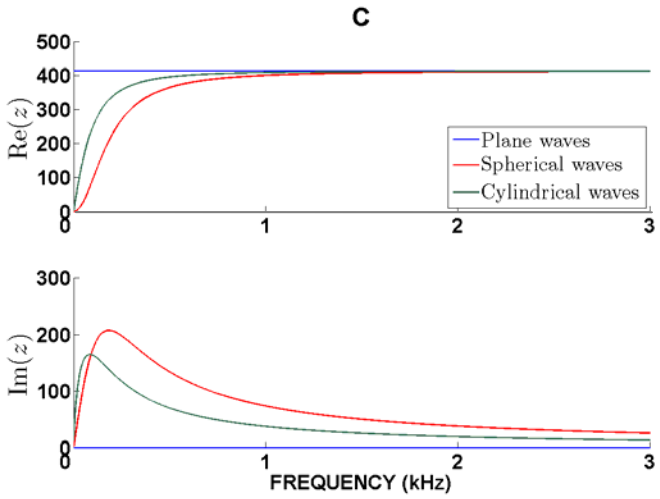

FIG. 7. C) Real and imaginary acoustic impedance as function of frequency for plane, cylindrical and spherical waves.

These simple cases support the reasoning that particle speed and sound pressure are linearly proportional. Adding all of above together with equation 2, it is found:

$$V_{air} \cong V \ \wedge \ p \cong aV \ \Rightarrow \ P(\omega) \cong aj\omega H(\omega)F(\omega)\,;\ (8)$$

The Lorentz force is proportional to the input current (at least for fixed θ); therefore, replacing $F(\omega) = bI(\omega)$ in relation *(8)* and normalizing constants ($ab = 1$) leads to a transfer function relating sound pressure to the time derivative of the current input:

$$H(\omega) \cong \frac{P(\omega)}{j\omega I(\omega)}\,;$$

REFERENCES

1. Shellock FG, Morisoli SM, Ziarati M. Measurement of acoustic noise during MR imaging: evaluation of six "worst-case" pulse sequences. Radiology 1994;191(1):91-93.

2. Haase A. Snapshot FLASH MRI. Applications to T1, T2, and chemical-shift imaging 3. Magn Reson Med 1990;13(1):77-89.

3. Hennig J, Nauerth A, Friedburg H. RARE imaging: a fast imaging method for clinical MR. Magn Reson Med 1986;3(6):823-833.

4. Mansfield P. Multi-Planar Image-Formation Using Nmr Spin Echoes. Journal of Physics C-Solid State Physics 1977;10(3):L55-L58.

5. Hedeen RA, Edelstein WA. Characterization and prediction of gradient acoustic noise in MR imagers. Magn Reson Med 1997;37(1):7-10.

6. Quirk ME, Letendre AJ, Ciottone RA, Lingley JF. Anxiety in patients undergoing MR imaging. Radiology 1989;170(2):463-466.

7. Bandettini PA, Jesmanowicz A, Van Kylen J, Birn RM, Hyde JS. Functional MRI of brain activation induced by scanner acoustic noise. Magn Reson Med 1998;39(3):410-416.

8. Cho Z, Chung S, Lim D, Wong E. Effects of the acoustic noise of the gradient systems on fMRI : A study on auditory, motor and visual cortices. 39 ed. 1998. 331-335.

9. McJury M, Stewart RW, Crawford D, Toma E. The use of active noise control (ANC) to reduce acoustic noise generated during MRI scanning: some initial results. Magn Reson Imaging 1997;15(3):319-322.

10. Mansfield P, Haywood B. Principles of active acoustic control in gradient coil design. MAGMA 2000;10(2):147-151.

11. Katsunuma A, Takamori H, Sakakura Y, Hamamura Y, Ogo Y, Katayama R. Quiet MRI with novel acoustic noise reduction. MAGMA 2002;13(3):139-144.

12. Rizzo S. CV, Versluis MJ, Hoogduin JM, Duifhuis H. Acoustc fMRI noise: Linear Time Invariant System model. IEEE Transactions on biomedical engineering. "in press". IEEE Xpress May. 2008.

13. Hennel F, Girard F, Loenneker T. "Silent" MRI with soft gradient pulses. Magn Reson Med 1999;42(1):6-10.

14. Hennel F. Fast spin echo and fast gradient echo MRI with low acoustic noise. J Magn Reson Imaging 2001;13(6):960-966.

15. Chen X, Shou X, Eagan TP, Brown R. Understanding acoustic noise suppression with gradient design: A vibrating string model. Proc. Int. Soc. Mag. Reson. Med. 16, 2988 (2008).

16. Chen X, Shou X, Derakhshan JJ, Shvartsman SM, Duerk JL, Brown RW. Experimental reduction of acoustic noise through cancellation of impulsive forces. Proc. Intl. Soc. Mag. Reson. Med. 16, 2962 (2008).

17. Eagan TP, Baig T, Derakhshan JJ, Duerk JL, Brown R. Acoustic noise suppression: Gradient self-help? Proc. Intl. Soc. Mag. Reson. Med. 15, 1101 (2007).

18. Gazdzinski C, Mechefske CK. Acoustic noise measurements in a 4T Whole-Body MRI scanner. Proc. Intl. Soc. Mag. Reson. Med. 10 (2002).

19. Mansfield P, Glover PM, Beaumont J. Sound generation in gradient coil structures for MRI. Magn Reson Med 1998;39(4):539-550.

20. Kinsler LE. Fundamentals of acoustics. John Wiley and Sons, Inc. 2000.

CHAPTER IV.

SUBJECTIVE LOUDNESS MEASURE OF fMRI ACOUSTIC NOISE[1]

Carlos V. Rizzo S, Dimitri Vrehen and Hendrikus Duifhuis

—Functional magnetic resonance imaging (fMRI) enables sites of brain activation to be localized in human subjects. For auditory system studies, however, the acoustic noise generated by the scanner tends to affect the activation significantly. The present study aims at a quantitative approach of noise reduction; we want to obtain physical and subjective magnitude measures of the acoustic scanner noise. This is achieved by performing a psychophysical matching experiment between three different echo planar imaging (EPI) sequences and a 1/3 octave band of pink noise, centered at 1 KHz. In nine subjects with normal hearing we found that the subjective measures of these six sounds do not increase linearly with the sound pressure levels (SPL) of the input signals. Sound signatures with lower damping factors and presented together are perceived louder than sound signatures with similar amount of energy but abruptly distributed, that is, displaying a more impulsive nature with higher separation and damping effects. EPI sequences with suppressed frequency components in the ear maximum sensitivity range and a highly impulsive discrete nature distributed over a longer time should be preferred for fMRI loudness reduction. In addition, gradient coil systems should place its resonance frequencies in the ear low sensitivity regions.

Index Terms—acoustic noise, fMRI, gradient noise, physical loudness, perceived loudness, SPL.

---

[1] Portions of this material were presented as traditional poster (923) at the 31st annual midwinter research meeting of the association for research in otolaryngology (ARO), February 16-21, 2008, Phoenix, Arizona, USA. In addition, a modified version of this manuscript is (in preparation) to be submitted for publication.

1. INTRODUCTION

FUNCTIONAL magnetic resonance imaging (fMRI) has successfully become an essential tool in human brain imaging since first proposed in 1990 (1, 2). But fMRI acoustic noise is a concern for the medical imaging and engineering community, since it exposes volunteers, patients, operators and medical practitioners to doses of high level sound for periods of time in the order of hours. Effects of this airborne sound exposure range from potential hearing loss to nonlinear effects on brain activation in patients and volunteers (3-7). Also, earplugs or other protectors which are worn by subjects (8) are not sufficient to achieve acceptable quiet conditions (9, 10). Every magnetic resonance (MR) scanner has its own acoustic transfer function characteristics mainly depending on its magnetic field strength and gradient coil system specifications; also each scanner has personalized sequences depending on its software parameters. However, typical fMRI acoustic noise has very special time waveform characteristics such as its impulsive nature and amplitude modulated carrier (11). Even though, scientific studies report fMRI acoustic noise in current scales such as sound pressure level (SPL) in dB, dB(A), equivalent continuous noise level (L_{eq}), and peak levels (L_{pk}); there is no accepted acoustical standard with a proper physical or subjective loudness scale for this type of impulse noise. Therefore, in this study we attempt to cover this gap by obtaining a subjective measure of fMRI scanner noise loudness using a psychophysical up and down matching experiment and comparing it to its current physical measure, using three different sound pressure levels for echo planar imaging (EPI) based scanner noise. Attempts to correlate both (subjective and current physical) fMRI acoustic noise loudness measures should lead to a better estimation, characterization and understanding of the effect of this type of noise in the human ear; also could elucidate a proper loudness scale related to this type of noise and eventually lead to its perceived reduction.

II. MATERIAL AND METHODS

The output sound of three different EPI sequences were recorded for 20 seconds each from a Philips Intera 3 Tesla MR scanner [maximum gradient strength 21 milliTesla(mT)/meter(m) per axis], located at the Behavioral and Cognitive Neurosciences (BCN) NeuroImaging Center (NiC) at the University of Groningen, The Netherlands. Additionally,

only for one EPI sequence (single shot gradient-echo) the input gradient coil currents in X, Y and Z directions were recorded using the same setup described later. This allowed the simulation of the output generated sound per three gradient coil directions for this sequence by multiplying (using the MATLAB signal analysis toolbox (R2007a)) input gradient current function times the already known MR scanner electro-acoustical transfer function per coil direction. Recording was taken while the helium coolant pump for the imager's permanent magnet was turned off. We employed a non-magnetic microphone support specially fitted to the edges of the patient's table inside the imager bore. Since the patient's table is indirectly coupled to the housing, the gradient coil cylinder is not directly coupled to the patient's table. Therefore, we expect that vibration cross-talk is limited to less than 1 dB. This was tested by measuring the sound field directly outside the bore. A more precise verification of this point requires simultaneous vibration measurement of the microphone housing, and is recommended for future research. To record sound inside the scanner a 1/2 inch condenser microphone Bruel Kjaer (B&K) 4190 (tested for MRI in (12)) was mounted on a non magnetic specially designed support and connected to a preamplifier (B&K ZC0026). Before measurements microphone and preamplifier were calibrated using sound level calibrator 4230 [B&K, ~94 dB at 1000 Hertz (Hz)]. This microphone and preamplifier are connected to a B&K Modular Precision Sound Analyzer 2260 through a 10 meter long extension cable (B&K AO0442). The 3T scanner used in this study supports a maximum current amplitude of approximately 700 Amperes (A), which can be read out using a manufacturer provided current monitor signal of 10 Volts (V), that is, 10V ≡ 700A, for each gradient coil X, Y and Z. Acquisition of the scanner gradient current monitor signal and of the microphone signal takes place via a 16 bits digital acquisition board (National Instruments 6052E) using LABVIEW 7.1 software (National Instruments 2004). Since no radio frequency (RF) signals are used for these measurements, a phantom was not needed, and the receiver RF head coil was removed from the scanner. All analog signals are low-pass filtered (Kemo Inc., 8-pole Bessel, cut-off frequency 14 kHz) before acquisition and some are sampled at 50 kHz and others at 44.1 kHz. All sound pressure recordings reported here were carried out at the scanner isocenter, which approximates the location where a human ear would be during scanning thereby giving an indication of the patient ear exposure. The

non-magnetic microphone support fitted to the edges of the patient's table inside the imager bore kept the microphone in a rigid horizontal position within a 1 mm range at the scanner isocenter. Sound pressure waveforms from EPI signals were derived from the recorded microphone output waveform using the microphone sensitivity [48.6 milliVolts (mV)/Pascal (Pa)]. For reference signal we employed a 1/3 octave band filtered pink noise (center frequency: 1 kHz). This noise was made using a physical noise generator (RG-1, T-0045, Wandel u.Goltermann. Reutlingen.Germany) creating pink noise which we fed into two successive filters (Model 3382 Filter 8 pole LP/HP Butterworth/Bessel, Krohn-Hite Corporation, USA), one high pass (cut off frequency: 891 Hz) and the other low pass (cut off frequency: 1120 Hz) both Butterworth types. This reference signal was recorded for 20 seconds using the same acquisition system at 50 kHz sampling frequency. The three different EPI noise (including 3 simulated EPI noise from X, Y and Z gradient coil direction) and reference signals are presented in a psychophysical up and down matching experiment inside a sound isolated booth to nine normal hearing subjects wearing headphones TDH-39 (10 Ohms Telephonics). The up and down matching experiment consists of presenting 250 ms of EPI noise (500 ms after space bar is pressed) followed by 250 ms of 1/3 octave band of filtered pink noise (center frequency = 1 kHz) separated each other by 100 ms of silence. After last sound is presented there is another 250 ms of silence just before the subject is asked which sound is perceived louder. The total auditory stimuli is presented in a 1350 ms length wave audio format (44100 Hz, 32-bit, Stereo, IEEE Float, 0.24 float type 3) generated using the MATLAB audio functions (R2007a). Sound is presented through national instruments data acquisition system (NIDAQ, PCI-6052E) by programmed analogue output channels coming from the connector block (NI SCB-68). The psychophysical experiment is conducted interactively using pre-calibrated headphone (TDH-39) by means of artificial ear type 4153 B&K with microphone 4190 B&K. One MATLAB algorithm loads the sound trains outside the cabin and two BNC cables from the SCB-68 analogue output deliver them into headphones inside booth. Subjects have to answer the question which sound was louder (either the first or the second) by pressing buttons "1 or 2" in a keyboard. The questions and sound delivery is performed by a MATLAB graphical user interface in a PC monitor inside the booth, which is controlled every time by pressing the space bar key. There is a total of 6 different

scanner noise played at three levels (60, 70 and 80 dB SPL) in order to match them with the reference noise. Reference noise starts approximately 15 dB SPL below the EPI noise level. The increasing or decreasing step size for the reference noise starts at +/- 4 dB. After the first 2 reversals or turning points, the step size is varied by +/- 2 dB. The system records 10 reversals per EPI noise level, but only employs the last eight to estimate the 50% of correct responses per EPI noise level and its standard deviation within 8 reversals per subject.

III. RESULTS AND DISCUSSION

Five (out of six) stimuli and reference signal in time and frequency domain are presented in figure 1 and 2, first and third column.

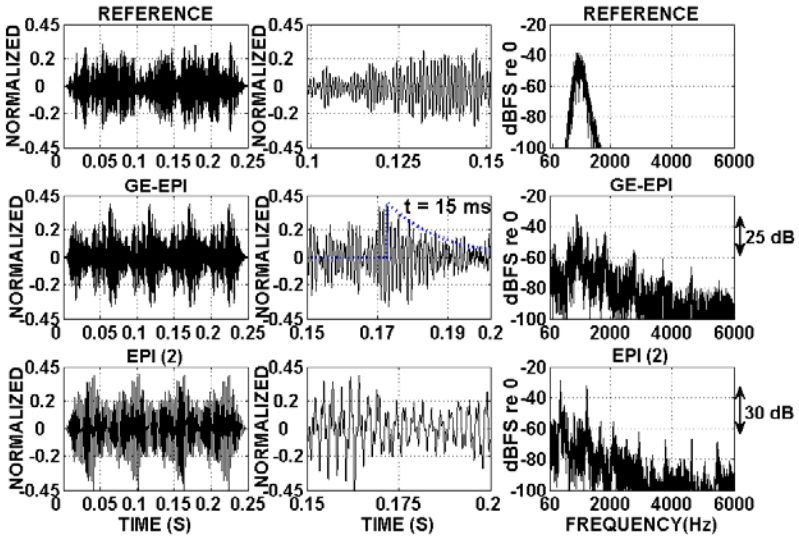

FIG. 1. Top row: Reference (filtered pink noise) waveform an amplitude spectrum. Middle and bottom row: Output acoustic waveform and amplitude spectra for two EPI sequences with higher loudness percept. Time waveforms close view of approximately 50 ms is included in second column. Dotted line represents decay time envelope for louder sequence: $0.4e^{-67t}$

Time waveforms close view of approximately 50 ms is included per stimuli and reference in second row. In figure 1 (middle and bottom row) the two sequences with highest loudness percept (70-80 dB SPL input range) are shown, whereas, figure 2 (middle and bottom row)

shows the two sequences with lowest loudness percept (70-80 dB SPL input range).

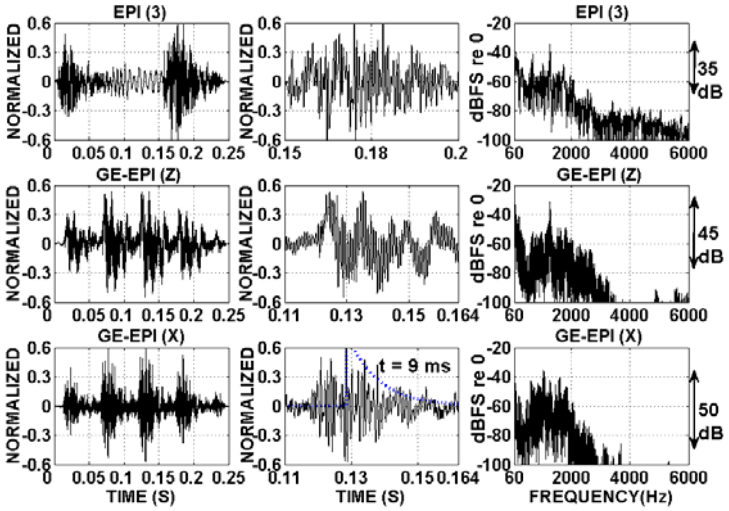

FIG. 2. Output acoustic waveform and amplitude spectra for three EPI sequences with lower loudness percept (top, middle and bottom row). Time waveforms close view of approximately 50 ms is included in second column. Dotted line represents decay time for quieter sequence: $0.75e^{-110t}$

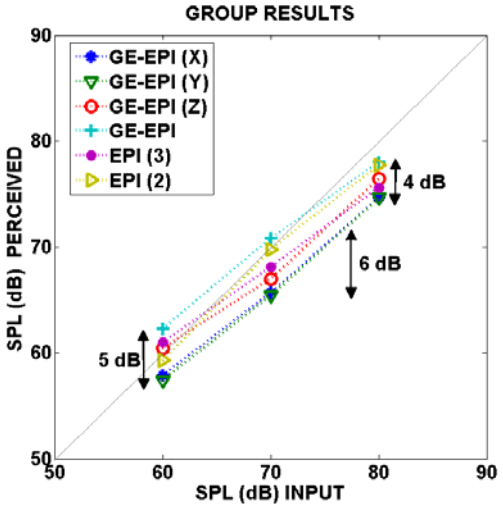

FIG. 3. Loudness percept related to reference versus input level (group results).

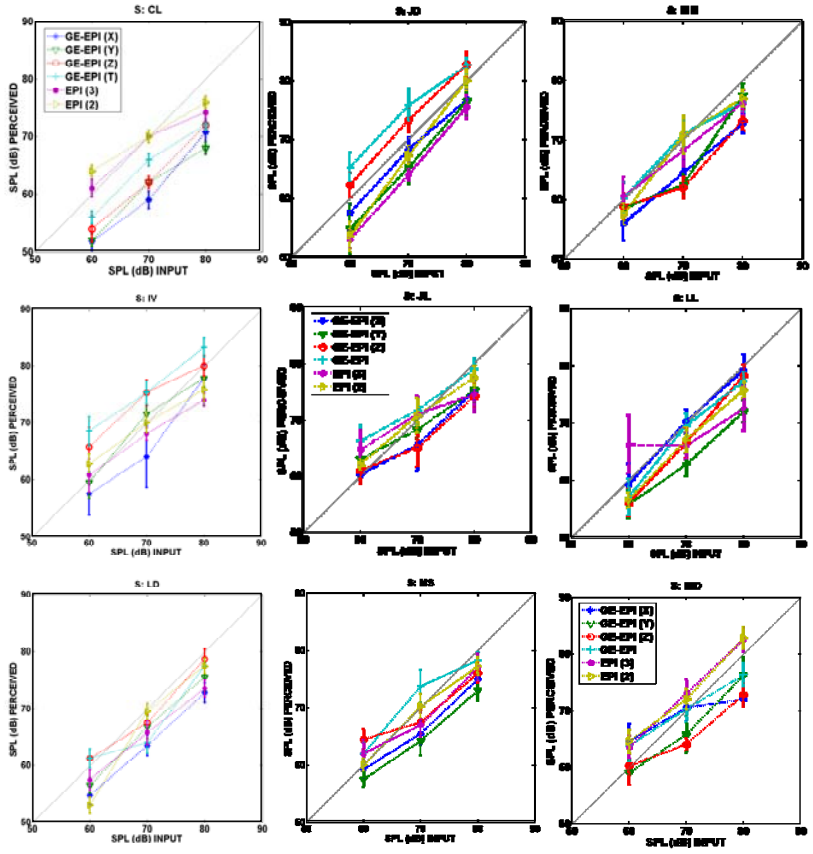

FIG. 4. Loudness percept related to reference versus input level (individual results).

Figure 3 shows the group results in loudness percept for 6 fMRI noise sequences referenced to 1/3 octave band of filtered pink noise (center frequency = 1 kHz). In nine subjects with normal hearing we found that the fMRI perceived loudness relative to reference signal does not increase linearly (figure 3) with the sound pressure level (SPL). The difference between the highest and lowest loudness percept sequence per increasing input level is 5, 6 and 4 dB SPL respectively (figure 3). This suggests a possible influence of basilar membrane nonlinearity on loudness perception, in particular for this type of fluctuating sound (13). It is possible that the loudness perception of fluctuating sounds would be affected by this fast-acting movement of the basilar membrane when loud MRI sound is perceived; in particular sounds with the same rms level but with different peak levels might have a

different loudness, since their effective excitation levels would differ after the movement ends. Also, the variation of basilar membrane movement with overall level could affect the loudness of modulated sounds such as fMRI acoustic noise. The two quietest sequences GE-EPI X, Z (figure 2 third column) present insignificant frequency components starting at 2.5 kHz more than 40 dB below the maximum amplitude spectrum; whereas the two loudest (figure 1, third column) sequences still present frequencies starting at 2.5 kHz around 25 dB below the maximum amplitude spectrum. Therefore, it is possible that frequencies in the 2.5 – 6 kHz range are responsible for a slight increase in fMRI loudness perception since this range coincides with the ear maximum sensitivity. Individual results for the nine subjects employed in this study are presented in figure 4. The loudness percept experiment is additionally repeated 8 times for two subjects; the stability of their individual results is shown in table I using the noise percept standard deviation (dB SPL) and the average standard deviation of the 50% correct response (dB SPL).

SEQUENCE TYPE	REFERENCE (σ)		50% RESPONSE AVG (σ)	
	I	II	I	II
GE-EPI (X) 60 dB	2.7	2.8	2.0	2.2
GE-EPI (X) 70 dB	2.6	2.5	2.6	2.1
GE-EPI (X) 80 dB	2.5	2.4	2.0	2.3
GE-EPI (Y) 60 dB	2.6	2.7	2.5	2.3
GE-EPI (Y) 70 dB	2.4	2.6	1.8	2.2
GE-EPI (Y) 80 dB	2.1	2.4	2.1	2.4
GE-EPI (Z) 60 dB	3.1	2.9	2.7	2.6
GE-EPI (Z) 70 dB	2.4	2.0	2.3	2.3
GE-EPI (Z) 80 dB	2.2	3.0	2.1	2.4
GE-EPI 60 dB	2.5	2.2	2.5	2.3
GE-EPI 70 dB	2.4	2.8	2.2	1.8
GE-EPI 80 dB	0.8	2.0	2.0	2.1
EPI (3) 60 dB	2.8	2.1	1.8	1.9
EPI (3) 70 dB	2.6	2.4	1.6	2.1
EPI (3) 80 dB	2.1	2.3	1.5	2.0
EPI (2) 60 dB	2.9	2.8	1.6	2.0
EPI (2) 70 dB	2.7	2.1	1.6	1.9
EPI (2) 80 dB	2.1	2.6	1.7	2.2

TABLE I. Psychophysical stability of two subjects (I and II) response across 8 repetitions. The three columns are scaled in dB SPL.

The decay time for the loudest (figure 1, middle row) and quieter (figure 2, bottom row) sequence is estimated by 15 and 9 ms

respectively. Their periodicity is similar in the order of 50 ms and related to the time acquisition per slice in this sequence. Damping effects seems to play a role in loudness perception of fMRI acoustic noise; this suggests that in addition to the total amount of energy in this type of stimuli, it matters how the energy is distributed over time. Figure 1 stimuli show a different energy distribution compared to figure 2 stimuli. Noise signatures with lower damping factors and less separated to each other (figure 1, first column) are perceived louder than noise signatures with similar amount of energy but abruptly distributed (figure 2, first column), that is, displaying a more impulsive nature with higher damping effects. This loudness percept underestimation is attributable to a less adaptation due to the discontinuous nature (impulsive nature) of the stimuli. Therefore, fMRI sequences with suppressed frequency components in the 2.5-6 kHz and highly impulsive nature distributed over a longer time should be preferred over more continuous noise signatures with less damping effects presenting frequency components in the range of ear maximum sensitivity. It was shown that noise signature periodicity was related to time selection per slice (14); additionally it was shown that slice thickness (proportional to time selection per slice) and SPL were inversely related for fMRI sequences (11). Therefore it is desirable for decreasing fMRI loudness perception to distribute the stimulus energy over a longer period by increasing the time selection per slice as much as possible. In addition, gradient coil systems should place its resonance frequencies in the ear low sensitivity regions. Further research should be carried out to estimate the loudness percept comparing different fMRI sequences from different facilities.

IV. CONCLUSION

Typical fMRI acoustic noise has a very special time waveform characteristics such as its impulsive nature and amplitude modulated carrier. Those characteristics suggest a possible influence of basilar membrane nonlinearity on its loudness perception. It is possible that the loudness perception of fMRI noise with the same rms level but with different peak levels is not equal, since their effective excitation levels would differ after the movement of the basilar membrane when loud MRI sound is perceived. Also, the variation of basilar membrane movement with overall level could affect the loudness of modulated sounds such as fMRI noise. Damping effects seems to play a role in loudness perception of fMRI acoustic noise; this suggests that in

addition to the total amount of energy in this type of stimuli, it matters how the energy is distributed over time. Noise signatures with lower damping factors and less separated to each other are perceived louder than noise signatures with similar amount of energy but abruptly distributed, that is, displaying a more impulsive nature with higher damping effects. Therefore, fMRI sequences with suppressed frequency components in the 2.5-6 kHz range and highly impulsive nature distributed over a longer time should be preferred over more continuous noise signatures with less damping effects presenting frequency components in the range of ear maximum sensitivity. It is desirable for decreasing fMRI loudness perception to distribute the stimulus energy over a longer period by increasing as much as possible the time selection per slice. In addition, gradient coil systems should place its resonance frequencies in the ear low sensitivity regions. Further research should be carried out to estimate the loudness percept using different fMRI sequences from different facilities.

REFERENCES

1. Ogawa S, Lee TM, Kay AR, Tank DW. Brain magnetic resonance imaging with contrast dependent on blood oxygenation. Proc Natl Acad Sci U S A 1990;87(24):9868-9872.

2. Mc Robbie DW. MRI from picture to proton. Cambridge, United Kingdom: University Press, 2003.

3. Brummett RE, Talbot JM, Charuhas P. Potential hearing loss resulting from MR imaging. Radiology 1988;169(2):539-540.

4. Bandettini PA, Jesmanowicz A, Van Kylen J, Birn RM, Hyde JS. Functional MRI of brain activation induced by scanner acoustic noise. Magn Reson Med 1998;39(3):410-416.

5. Cho Z, Chung S, Lim D, Wong E. Effects of the acoustic noise of the gradient systems on fMRI : A study on auditory, motor and visual cortices. 39 ed. 1998. 331-335.

6. Elliott MR, Bowtell RW, Morris PG. The effect of scanner sound in visual, motor, and auditory functional MRI. Magn Reson Med 1999;41(6):1230-1235.

7. Mazard A, Mazoyer B, Etard O, Tzourio-Mazoyer N, Kosslyn SM, Mellet E. Impact of fMRI acoustic noise on the functional anatomy of visual mental imagery. J Cogn Neurosci 2002;14(2):172-186.

8. Savoy R. The Psychophysical laboratory in the magnet: Stimulus delivery , Response recording, and safety, in medical radiology, Diagnostic Imaging and radiation oncology: Functional MRI. Berlin: Springer, edited by C. Moonen and P. Bandettini , pp. 347-365. 1999..

9. Ravicz ME. Reducing imager generated noise at the ear during functional magnetic resonance imaging: Passive attenuation, Abstracts of the twenty first midwinter meeting of the association for research in otolaryngology (ARO, Mt. Royal, NJ), p. 208. 1998.

10. Ravicz ME. Imager noise and noise reduction during fMRI, Neuroimage 7 (4) , S556. 1998b.

11. Counter SA, Olofsson A, Borg E, Bjelke B, Haggstrom A, Grahn HF. Analysis of magnetic resonance imaging acoustic noise generated by a 4.7 T experimental system. Acta Otolaryngol 2000;120(6):739-743.

12. Gazdzinski C, Mechefske CK. Acoustic noise measurements in a 4T Whole-Body MRI scanner. Proc. Intl. Soc. Mag. Reson. Med. 10 (2002).

14. Rizzo S. CV, Versluis MJ, Hoogduin JM, Duifhuis H. Acoustc fMRI noise: Linear Time Invariant System model. IEEE Transactions on biomedical engineering. "in press".

CHAPTER V.

SOUND ENCLOSURE EFFECTS IN MRI ACOUSTIC CHARACTERIZATION[1]

Carlos V. Rizzo S and Hendrikus Duifhuis

—Electro-acoustical characterization of one magnetic resonance imaging (MRI) gradient coil system was studied in six different locations inside and outside the scanner bore. We want to obtain qualitative and quantitative effects of MRI bore enclosure in electro-acoustical transfer function estimation. This is achieved by estimating the gradient coil system resonance frequencies and reverberation time at different locations. The same two main resonance frequencies per coil are found to be maxima at all six transfer function gain locations. Across different coils, the X and Y direction present common transfer function gain maxima around 648 Hz (mean value) and 1073 Hz (mean value). The former is expected to represent the gradient coil bending mode shape or so called banana-shape mode of the vibrating structure. The Z direction coil presents transfer function gain maxima around 1274 Hz and 1554 Hz; the former (1274 Hz) is expected to represent the gradient coil radial mode shape or so called cone-shape mode of the vibrating structure. The overall reverberation time and electro-acoustical transfer function shape per coil is to some extent comparable in all locations. These findings suggest a minimum MRI bore enclosure effect in electro-acoustical transfer function estimation for our facility.

Index Terms—acoustic noise, enclosure acoustics, fMRI, gradient noise, reverberation time, SPL.

[1] A modified version of this manuscript is (in preparation) to be submitted for publication.

I. INTRODUCTION

MAGNETIC resonance imaging (MRI) scanners are widely used in hospitals for both medical diagnosis and clinical research. Magnetic field strengths as high as 1 Tesla (T) or more are common, allowing a high spatial imaging resolution using fast scanning sequences. However, the acoustic noise generated during scanning increases with higher magnetic field strength. The way that the magnetic field must be manipulated during the scanning process causes significant vibrations of the gradient coil (a cylindrical electro-magnet which produces a spatially varying magnetic field) and therefore acoustic noise levels to be generated within and nearby the scanners. The acoustic noise reported (1) varied from 85 dB(A) for 0.2 – 0.5T systems to 115 dB(A) for 3T systems. However, Price et al. also point out that noise levels reach up to 130 dB(A) for 3T systems with the new increase in slew rates (1). One of the highest sound pressure levels (SPL) recorded reached up to 138 dB in a 3T imager with echo planar imaging (EPI) sequences (2). In another 4.7T system (3), the highest sound pressure level was observed at 130 dB(A) using rapid acquisition with enhancement sequences. The high levels of acoustic noise present problems to patients and health care workers in the form of annoyance, anxiety and long term hearing damage. In previous studies (4, 5) of the acoustic scanner noise it has been proposed that the physical structure of the MR scanner behaves as a linear time invariant (LTI) electro-acoustical system where gradient coil currents $I(t)$ can be interpreted as input and generated sound pressure signals $p(t)$ as outputs of the LTI-system. Physically, the system is made of the mechanical structure of the MR scanner, including magnet, gradient coils, RF body coil, support structures and the structure of the acoustic space inside the body coil where the patient would typically be exposed to the noise. The MRI electro-acoustical transfer function characterizes the system and is a first step in modeling and predicting MRI acoustic noise (4, 6). Additionally, by avoiding gradient coil system resonance frequencies the scanner experiences a substantial acoustic noise reduction (7). Although, MRI electro-acoustical transfer function characterization was first proposed in 1997 (4), there are no studies assessing the variability of that estimation inside and outside the scanner bore, that is assessing the effects of the MRI bore

enclosure. However, Kuijpers et al describes MRI noise radiation models inside the MRI bore and it discusses briefly about possible minor room effects in MRI noise radiation (8). Therefore, we attempt to estimate enclosure effects in this transfer function main resonance peaks by computing transfer function in a total of 6 locations along the operator room direction, three locations inside and three outside the bore. The idea that acoustic reverberation plays a role in MRI electro-acoustical transfer function will be investigated by overall reverberation time (9) estimation for the same locations.

II. MATERIAL AND METHODS

The experiment was performed on a Philips Intera 3 Tesla MR scanner [maximum gradient strength 21 milliTesla(mT)/meter(m) per axis], located at the Behavioral and Cognitive Neurosciences (BCN) NeuroImaging Center (NiC) at the University of Groningen, The Netherlands. We employed a non-magnetic microphone support specially fitted to the edges of the patient's table inside the imager bore. Since the patient's table is indirectly coupled to the housing, the gradient coil cylinder is not directly coupled to the patient's table. Therefore, we expect that vibration cross-talk is limited to less than 1 dB. This was tested by measuring the sound field directly outside the bore. A more precise verification of this point requires simultaneous vibration measurement of the microphone housing, and is recommended for future research. To record sound inside the scanner a 1/2 inch condenser microphone Bruel Kjaer (B&K) 4190 (tested for MRI in (10)) was mounted on a non magnetic specially designed support and connected to a preamplifier (B&K ZC0026). Before measurements microphone and preamplifier were calibrated using sound level calibrator 4230 [B&K, ~94 dB at 1000 Hertz (Hz)]. This microphone and preamplifier are connected to a B&K Modular Precision Sound Analyzer 2260 through a 10 meter long extension cable (B&K AO0442). The 3T scanner used in this study supports a maximum current amplitude of approximately 700 Amperes (A), which can be read out using a manufacturer provided current monitor signal of 10 Volts (V), that is, 10V ≡ 700A, for each gradient coil X, Y and Z. Acquisition of the scanner gradient current monitor signal and of the microphone signal takes place via a 16 bits digital acquisition board (National Instruments 6052E) using LABVIEW 7.1 software (National Instruments 2004). Since no radio frequency (RF) signals are used for these measurements, a phantom was not needed,

and the receiver RF head coil was removed from the scanner. All analog signals are low-pass filtered (Kemo Inc., 8-pole Bessel, cut-off frequency 14 kHz) before acquisition and are sampled at 50 kHz; The data were analyzed using the MATLAB signal analysis toolbox (R2006a).

From the different excitation methods that can be used to estimate the MR scanner transfer function (calibration), such as broadband noise, pulses, and frequency sweeps, we selected the pulse excitation method. Therefore, one input sequence was recorded with the generated output sound, while the helium coolant pump for the imager's permanent magnet was turned off. That is, a calibration trapezoidal pulse [0.1 milliseconds (ms) raise and fall time, 0.01 ms plateau time, 10 mT/m amplitude] was presented to the X-gradient coil at 0.5 seconds (s) intervals for 10 seconds. This procedure was repeated for Y and Z gradients. Additionally, 10 seconds of background noise (air-handling system) was recorded for reference. All sound pressure recordings reported here started at the scanner isocenter, (location 1 in figure 8, which approximate the location where a human ear would be during scanning thereby giving an indication of the patient ear exposure) and were extended to five more locations inside and outside the MRI bore (locations 2 to 6 in figure 8). The non-magnetic microphone support fitted to the edges of the patient's table inside the imager bore kept the microphone in a rigid horizontal position within a 1 mm range of the desired location. Five more locations were measured at the patient's table along the operator room (Z) direction. That is two inside the bore, 25 cm and 75 cm respectively from the isocenter (at its same height 1 m approximately). Three locations outside the bore 90 cm, 190 cm and 230 cm respectively from isocenter, at same isocenter height (points 4 to 6 in figure 7). The input gradient currents for calibration pulses were recorded by the acquisition system. Sound pressure waveforms generated by calibration were derived from the recorded microphone output waveform using the microphone sensitivity [48.6 milliVolts(mV)/Pascal(Pa)]. Given the response pressure (in Pa) and the time derivative of the stimulus input current (in A/s), the transfer function (11) is computed for each gradient coil taking the (complex) ratio of response spectrum over input spectrum. This is computed for each pulse and then averaged across 19 pulses. One 0.5 s Kaiser window, β =11 (12) centered at the stimulus peak, was used for

optimal processing of stimuli and responses. In the present study the pulse excitation up to 8 kHz was used to estimate the transfer function. A 10 s background noise signal is also filtered within the auditory range by means of a 2nd order Butterworth digital filter (sampling frequency 50 kHz, 25000 sample points, cutoff frequency 6 Hz and exponentially time averaged (13) (using 125 ms time constant equivalent to the Fast (F) sound level meter settings which use a resistor-capacitor RC time of 125 ms) over 0.5 s samples.

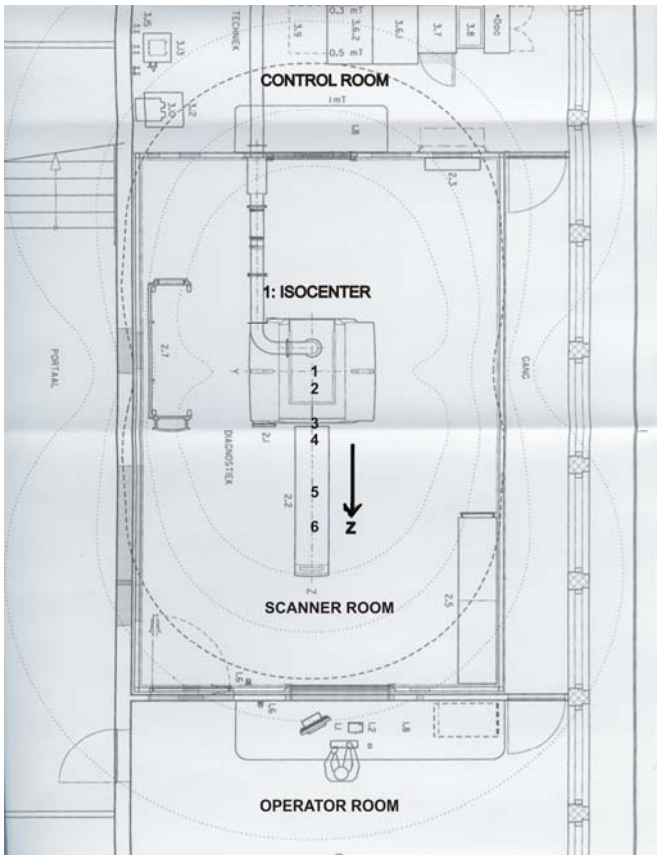

FIG. 8. Upper view of six measurement points in the MRI scanner room along the operator room (Z) direction: Locations 1,2,3 inside the bore and 4,5,6 outside bore.

The sample with maximum root-mean-square (RMS) pressure is taken and its amplitude spectrum is estimated after applying the Kaiser

window specified above. The impulse response per location is obtained by inverse fast Fourier transform of the X, Y and Z transfer functions over the 500 Hz to 8000 Hz range. The overall reverberation time[2] estimation was obtained from the linear approximation of the absolute value of the impulse response on a logarithmic (dB) scale.

III. RESULTS AND DISCUSSION

Transfer function gain and impulse response estimations at six different locations are presented in figures 1 to 3 and 4 to 6 respectively, per gradient coil direction. The total background noise sound pressure level (SPL) is 64 dB and found to be somewhat constant in all measurement locations. The same two main resonance frequencies per coil are found to be maxima at all six transfer function gain locations, shown within dotted lines in figures 1, 2 and 3.

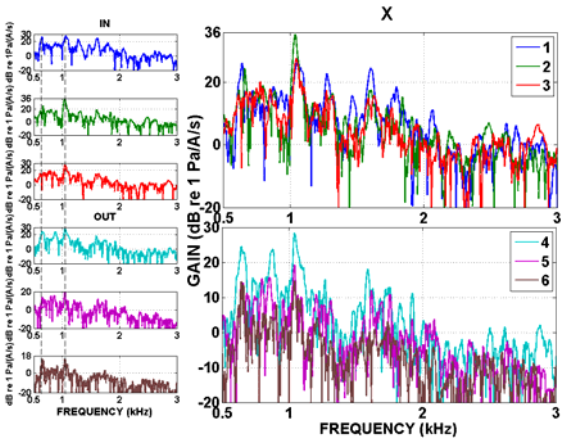

FIG. 1. Left: Six individual electro-acoustical transfer function gains (X coil) showing same two main resonance frequencies. (Top): Three locations inside MRI bore (1,2,3). (Bottom): Three locations outside MRI bore (4,5,6). Right: Group electro-acoustical transfer function gains showing inside bore locations (Top) and outside bore locations (Bottom).

That is 642 Hz and 1058 Hz for X coil (figure 1); 654 Hz and 1088 Hz for Y coil (figure 2), 1274 Hz and 1554 Hz for Z coil (figure 3). Based

[2] Reverberation time, defined as the time required for the sound level to drop by 60 dB.

on the concept of structural mode shapes (14) a large number of structural modes exist for the gradient coil cylindrical assembly.

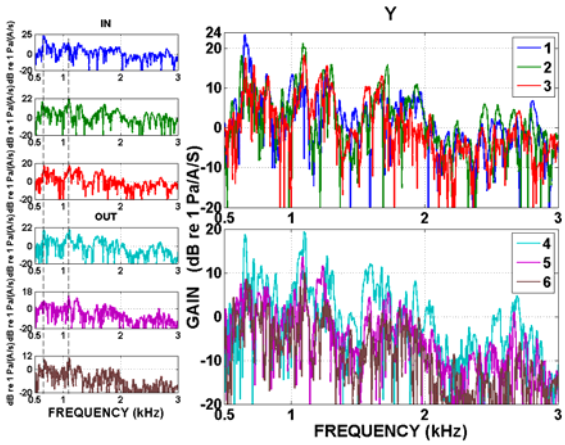

FIG. 2. Left: Six individual electro-acoustical transfer function gains (Y coil) showing same two main resonance frequencies. (Top): Three locations inside MRI bore (1,2,3). (Bottom): Three locations outside MRI bore (4,5,6). Right: Group electro-acoustical transfer function gains showing inside bore locations (Top) and outside bore locations (Bottom).

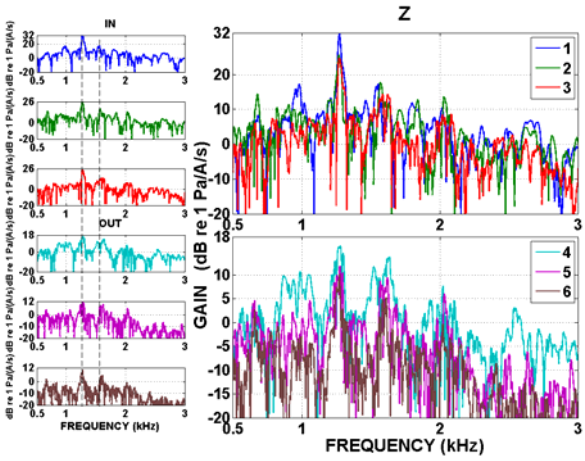

FIG. 3. Left: Six individual electro-acoustical transfer function gains (Z coil) showing same two main resonance frequencies. (Top): Three locations inside MRI bore (1,2,3). (Bottom): Three locations outside MRI bore (4,5,6). Right: Group electro-acoustical transfer function gains showing inside bore locations (Top) and outside bore locations (Bottom).

However, since the Lorentz forces acting upon the gradient coil windings set the gradient coil structure into vibration, only a few modes of the gradient coil structure are excited due to the specific spatial distribution of these forces (figure 7)**.**

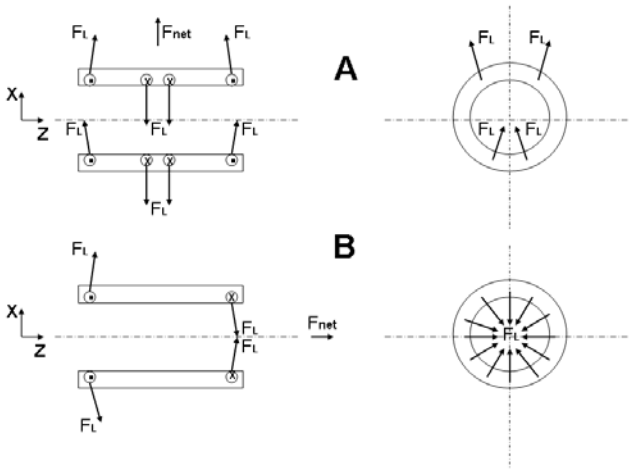

FIG. 7. Lorentz force (FL) and net force (Fnet) distribution in the X-(A) and Z-coil windings (B), transversal and frontal view.

Across different coils in our facility, the X and Y direction present common transfer function gain maxima around 648 Hz (mean value) and 1073 Hz (mean value). The former is expected to represent the so called banana-shape (transversal) bending mode of the vibrating structure (15-18). The Z direction coil presents transfer function gain maxima around 1274 Hz and 1554 Hz; the former (1274 Hz) is expected to represent the so called cone-shape (radial) mode of the vibrating structure as well (15-18). The electro-acoustical transfer function shape per coil is comparable to each other in the three locations inside the MRI bore. Although, the electro-acoustical transfer function shape per coil outside the bore is to some extent comparable to each other, they present somewhat dissimilarities in shape compared to the ones estimated inside the bore (see column of figures 1, 2 and 3 respectively). These differences could be due to lower signal to noise ratio as the measurement location is further away from the noise source. The impulse response estimation per coil (figures 4, 5 and 6) is to some extent comparable to each other inside and outside the bore locations.

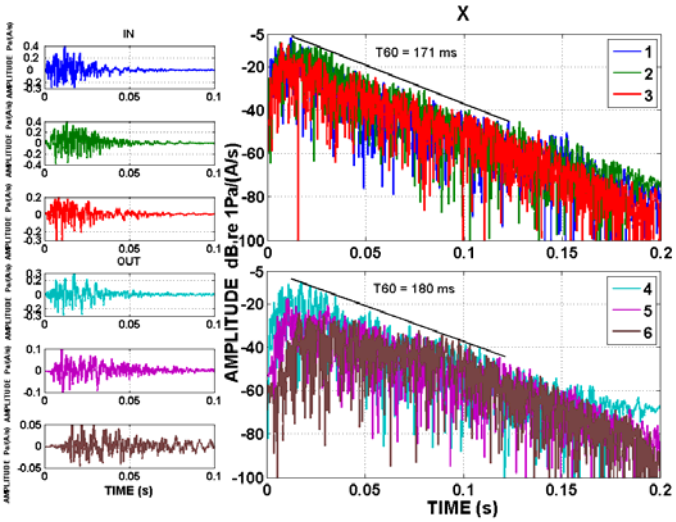

FIG. 4. Left: Six individual impulse responses (X coil) showing three locations inside (Top) MRI bore (1,2,3) and three locations outside (Bottom) bore (4,5,6). Right: Absolute value of the impulse response on a logarithmic (dB) showing inside bore locations (Top) and outside bore locations (Bottom).

Some differences could rise due to lower signal to noise ratio and time delays for the measurement locations away from the noise source compared to the ones closer (inside bore). The overall reverberation time per coil (X, Y and Z) is comparable in all locations: 170 ms, 210 ms and 170 ms, inside bore locations. For outside bore locations per coil (X, Y and Z) the following reverberation time is found: 180 ms, 240 ms and 189 ms, respectively. Minor differences are seen in locations outside MRI bore (compared to the ones inside bore) due to longer build up time because of time delay in noise propagation. Therefore, longer reverberation times (across coils) were estimated for outside locations compared to inside locations. The reverberation time variation between inside and outside bore locations (within coils) are also comparable to each other, 10 ms, 30 ms and 19 ms, for X, Y and Z respectively. The overall reverberation time per gradient coil (in the order of 200 ms) is very short to play a determinant role during functional imaging acoustic noise. In addition, a technique called sparse imaging (19) in which functional images are not acquired continuously, but separated by relatively long periods of scanner inactivity approximately 10 s. is introduced to reduce the effect of scanner noise on the measured signals. The estimated reverberation

time is a factor of 50 smaller than silent periods during sparse temporal sampling.

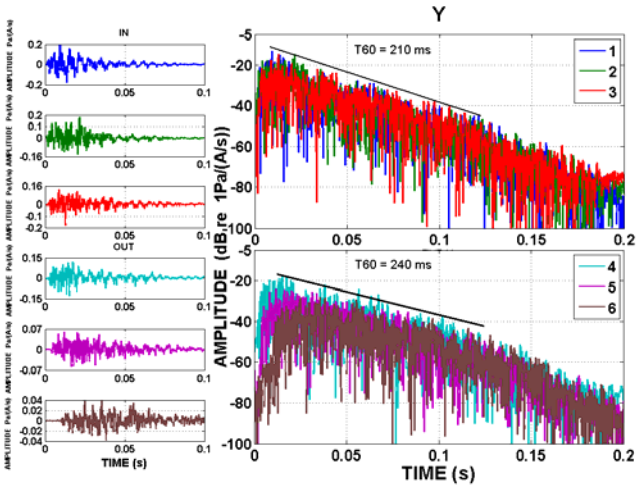

FIG. 5. Left: Six individual impulse responses (Y coil) showing three locations inside (Top) MRI bore (1,2,3) and three locations outside (Bottom) bore (4,5,6). Right: Absolute value of the impulse response on a logarithmic (dB) showing inside bore locations (Top) and outside bore locations (Bottom).

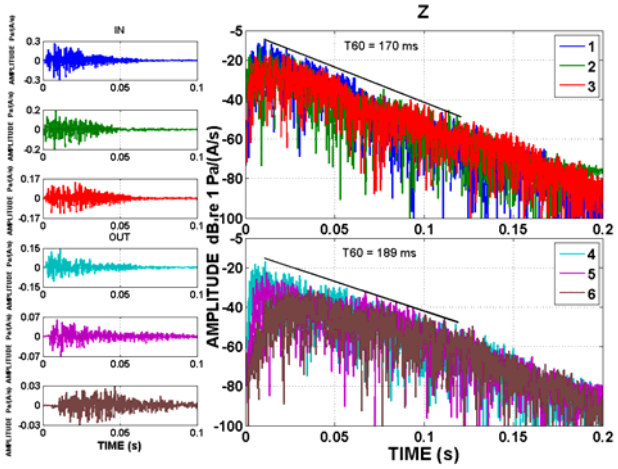

FIG. 6. Left: Six individual impulse responses (Z coil) showing three locations inside (Top) MRI bore (1,2,3) and three locations outside (Bottom) bore (4,5,6). Right: Absolute value of the impulse response on a logarithmic (dB) showing inside bore locations (Top) and outside bore locations (Bottom).

The transfer function gain does not present visible differences in two main resonance peaks per coil (as shown before). In addition, the overall reverberation time is comparable for all locations across the three different gradient coils (within maximum 30 ms difference for Y coil inside and outside locations); these two findings suggests a minimum MRI bore enclosure effect in electro-acoustical transfer function estimation for our facility. However, further research on MRI acoustic noise characterization should include estimation of enclosure effects parameters such as reverberation time per frequency inside and outside the MRI. Figures 9 to 11 show the gradient coil acoustic amplitude variation for four frequencies as a function of longitudinal direction, displaying the six measurement locations. Within the X, Y and Z coil, the amplitude of the four frequency components show a decreasing tendency with distance for the three inside and three outside bore locations, whereas, the 4000 Hz component shows this behavior in a more abrupt way for X and Y coils (figures 9 and 10). Across different coils, the amplitude maximum variation of the frequency components range between 15 and 30 dB. That is, a 13 dB maximum variation along the longitudinal distance for the 500 Hz frequency, 20 dB for 1000 Hz, 30 dB for the 2000 Hz frequency and 25 dB maximum variation for 4000 Hz, respectively.

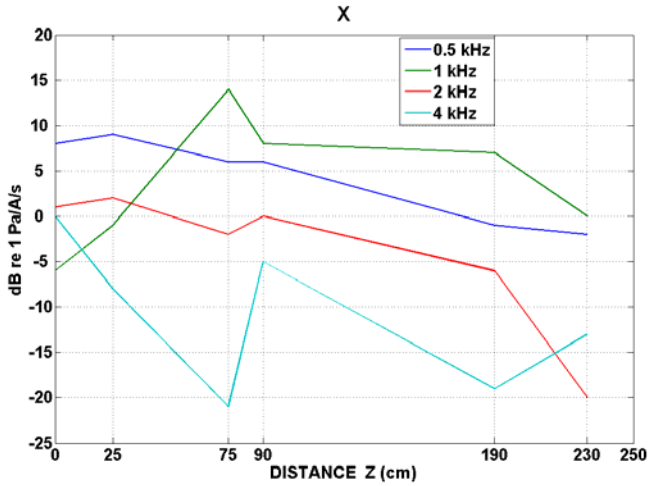

FIG. 9. X gradient coil acoustic amplitude variation (four frequencies) as a function of longitudinal direction, displaying six measurement locations.

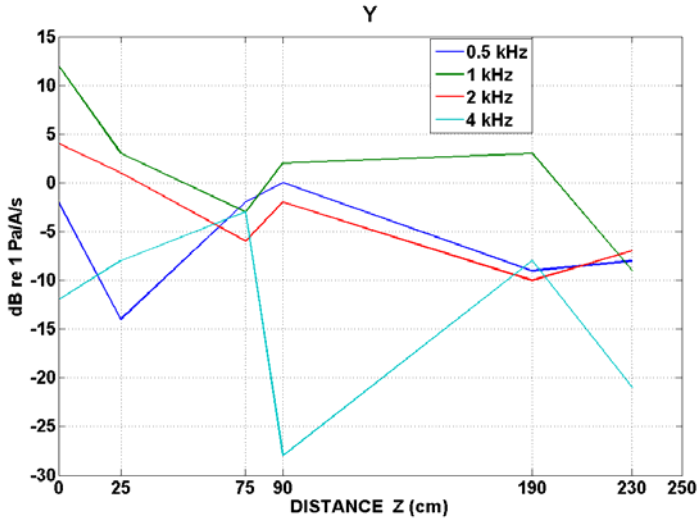

FIG. 10. Y gradient coil acoustic amplitude variation (four frequencies) as a function of longitudinal direction, displaying six measurement locations.

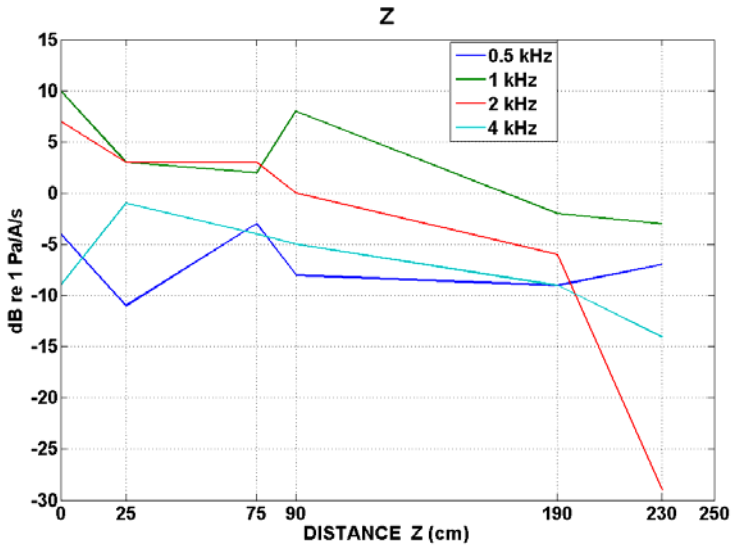

FIG. 11. Z gradient coil acoustic amplitude variation (four frequencies) as a function of longitudinal direction, displaying six measurement locations.

IV. CONCLUSION

Electro-acoustical characterization of one magnetic resonance imaging (MRI) gradient coil system was studied in six different locations inside and outside the scanner bore. The same two main resonance frequencies per coil are found to be maxima at all six transfer function gain locations. Across different coils, the X and Y direction present common transfer function gain maxima around 648 Hz (mean value) and 1073 Hz (mean value). The former is expected to represent the so called banana-shape (transversal) mode of the vibrating structure. The Z direction coil presents transfer function gain maxima around 1274 Hz and 1554 Hz. The former (1274 Hz) is expected to represent the so called cone-shape (radial) mode of the vibrating structure. The overall reverberation time (in the order of 200 ms) and electro-acoustical transfer function shape per coil is to some extent comparable in all locations. Minor differences are due to signal to noise ratio and time delays associated to locations far away (outside MRI bore) from noise source. These findings suggest a minimum MRI bore enclosure effect in electro-acoustical transfer function estimation for our facility. However, further research on MRI acoustic noise characterization should include estimation of enclosure effects parameters such as reverberation time per frequency inside and outside the MRI.

ACKNOWLEDGMENT
The authors would like to thank PhD candidate Maarten J. Versluis for programming the MRI calibration pulse signal and also appreciate his cooperation during recording sessions.

REFERENCES

1. Price DL, De Wilde JP, Papadaki AM, Curran JS, Kitney RI. Investigation of acoustic noise on 15 MRI scanners from 0.2 T to 3 T. J Magn Reson Imaging 2001;13(2):288-293.

2. Ravicz ME, Melcher JR, Kiang NY. Acoustic noise during functional magnetic resonance imaging. J Acoust Soc Am 2000;108(4):1683-1696.

3. Counter SA, Olofsson A, Borg E, Bjelke B, Haggstrom A, Grahn HF. Analysis of magnetic resonance imaging acoustic noise generated by a 4.7 T experimental system. Acta Otolaryngol 2000;120(6):739-743.

4. Hedeen RA, Edelstein WA. Characterization and prediction of gradient acoustic noise in MR imagers. Magn Reson Med 1997;37(1):7-10.

5. Barnett A. Comments on "gradient-induced acoustic and magnetic field fluctuations in a 4T whole-body MR imager". Magn Reson Med 2001;46(2):207.

6. Li W, Mechefske CK. Acoustic Noise Analysis and Prediction in a 4-T MRI scanner" Concepts in Magnetic Resonance Part B (Magnetic Resonance Engineering) Vol. 21B(1): 19-25, 2004.

7. Tomasi DG, Ernst T. Echo planar imaging at 4 Tesla with minimum acoustic noise. Journal of Magnetic Resonance Imaging 2003;18(1):128-130.

8. Kuijpers AH. Acoustic modeling and design of MRI scanners. PhD thesis. Technical University Eindhoven. 1999.

9. Kinsler LE. Fundamentals of acoustics. John Wiley and Sons, Inc. 2000.

10. Gazdzinski C, Mechefske CK. Acoustic noise measurements in a 4T Whole-Body MRI scanner. Proc. Intl. Soc. Mag. Reson. Med. 10 (2002).

11. McClellan JH, Schafer RW, Yoder, M. A. Signal Processing First. Pearson Prentice Hall. 2003. International edition. Chapters 5, 6 and 10.

12. Hayes MH. Schaum's outline of theory and problems of digital signal processing. Mc-Graw Hill companies Inc. 1999. Chapter 9, p 361.

13. Beranek LL. Acoustical Measurements. Acoustical Society of America 1988. Chapter 20.

14. Gawronski WK. Advanced Structural Dynamics and Active control of Structures. New York: Springer-Verlag, 2004.

15. Hoiting GJ. "Measuring MRI noise". PhD Thesis, 2005. ISBN 90-367-2235-7 (Online version).

16. Roozen NB, Philips PPH, Biloen D, Limpens P, Tuithof HH. Active vibration isolation applied to a magnetic resonance imaging (MRI) system. Twelfth International congress on sound and vibration. Lisbon, 2005.

17. Roozen NB, Koevoets AH, den Hamer AJ. Active vibration control of gradient coils to reduce acoustic noise of MRI systems. IEEE/ASME Transactions on mechatronics, VOL. 13, No. 3, JUNE 2008.

18. Tomasi D, Ernst T. A simple theory for vibration of MRI gradient coils. Brazilian Journal of Physics, vol. 36, no. 1A, March, 2006.

19. Hall DA, Haggard MP, Akeroyd MA, Palmer AR, Summerfield AQ, Elliott MR, Gurney EM, Bowtell RW. "Sparse" temporal sampling in auditory fMRI. Hum Brain Mapp 1999;7(3):213-223.

CHAPTER VI.

SUMMMARY

Functional magnetic resonance imaging (fMRI) enables sites of brain activation to be localized in human subjects. For auditory system studies, however, the acoustic noise generated by the scanner tends to interfere with the assessments of this activation. Understanding and modeling fMRI acoustic noise is a useful step to its reduction. To study acoustic noise the MR scanner is modeled as a linear electro-acoustical system in **chapter 2** generating sound pressure signals proportional to the time derivative of the input gradient currents. The transfer function of one MR scanner is determined for two different input specifications: (1) by using the gradient waveform calculated by the scanner software, and (2) by using a recording of the gradient current. Up to 4 kHz the first method is shown as reliable as the second one, and its use is encouraged when direct measurements of gradient currents are not possible. Additionally, the linear order and average damping properties of the gradient coil system are determined by impulse response analysis. Since fMRI is often based on echo planar imaging (EPI) sequences, a useful validation of the transfer function prediction ability can be obtained by calculating the acoustic output for the EPI sequence. We found a predicted sound pressure level (SPL) for the EPI sequence of 104 decibels (dB) SPL compared to a measured value 102 dB SPL. As yet, the predicted EPI pressure waveform shows similarity as well as some differences with the directly measured EPI pressure waveform.

A method to reduce the acoustic noise generated by gradient systems in magnetic resonance imaging (MRI) is proposed in **chapter 3** based on the linear response theory: destructive interference of resonance frequencies. Since the physical cause of MRI acoustic noise is the time derivative of the gradient current, a common trapezoid current shape only excites the gradient in the rising and falling edge. In the falling edge the coil is excited with 180 degree phase difference with respect to rising edge. Therefore, by varying the width of the trapezoid and keeping the ramps constant, it is possible to suppress one selected

frequency and its higher harmonics. This value is matched to one of the prominent resonance frequency of the gradient coil system. The idea of cancelling a single frequency is extended to a second frequency using two successive trapezoid shape pulses presented at a selected interval. Sound pressure level (SPL) reduction of 6 and 10 dB is found for the two trapezoid shapes and a single pulse shape, respectively. The proposed pulse shapes are additionally tested in a simulated echo planar imaging (EPI) read out train obtaining SPL reduction of 12 dB for the best case.

The study in **chapter 4** aims at a quantitative approach of noise reduction; we want to obtain physical and subjective magnitude measures of the acoustic scanner noise. This is achieved by performing a psychophysical matching experiment between five different echo planar imaging (EPI) sequences and a 1/3 octave band of pink noise, centered at 1 KHz. Additionally, three simulated noise signals (for one EPI sequence) produced by x, y and z gradient coil direction respectively were matched with the 1/3 octave band of pink noise. In nine subjects with normal hearing we found that the subjective measures of these 6 sounds do not increase linearly with the sound pressure levels (SPL) of the input signals. This study supports our working hypothesis that as long as we do not have a full understanding of the relation between the acoustic properties of EPI noise and its subjective percept, its characterization and the estimated subjective effects should consist of both (physical and subjective measures). The implication is that for development of an effective fMRI acoustic noise reduction technique the perceived (subjective) loudness characteristics of this noise should be more extensively studied and combined with well known physical magnitudes given by current sound analyzer technology.

Electro-acoustical characterization of one magnetic resonance imaging (MRI) gradient coil system in **chapter 5** was studied in six different locations inside and outside the scanner bore. We want to obtain qualitative and quantitative effects of MRI bore enclosure in electro-acoustical transfer function estimation. This is achieved by estimating the gradient coil system resonance frequencies and reverberation time at different locations. The same two main resonance frequencies per coil are found to be maxima at all six transfer function gain locations. Across different coils, the X and Y direction present common transfer

function gain maxima around 648 Hz (mean value) and 1073 Hz (mean value). The former is expected to represent the gradient coil bending mode shape or so called banana-shape mode of the vibrating structure. The Z direction coil presents transfer function gain maxima around 1274 Hz and 1554 Hz. The former (1274 Hz) is expected to represent the gradient coil radial mode shape or so called cone-shape mode of the vibrating structure. The overall reverberation time and electro-acoustical transfer function shape per coil is comparable to some extent in all locations. These findings suggest a minimum MRI bore enclosure effect in electro-acoustical transfer function estimation for our facility.

SAMENVATTING

Functional magnetic resonance imaging (fMRI) maakt het mogelijk actieve gebieden in de hersenen to localiseren. Echter, bij de bestudering van het auditieve system is er een gerede kans dat het door de scanner gegenereerde geluid de bepaling van deze actieve gebieden direct beinvloed. Een nuttige stap in de minimaliseren van die invloed bestaat in het analyseren en modelleren van dit stoorgeluid. Om het door gegenereerde geluid te analyseren wordt in hoofdstuk 2 de MR-scanner gemodelleerd als een elektro-akoestisch systeem dat een geluidsdruk genereert die evenredig is met de tijdafgeleide van de input-gradient-stromen. De overdrachtsfunctie van en MR-scanner is bepaald voor twee verschillende input-specificaties: (1) gebruik makend van de gradientgolfvorm die berekend wordt door de scannersoftware, en (2) door gebruik te maken van gemeten gradientstroom. Voor frequenties tot 4 kHz blijkt de eerste methode even betrouwbaar als de tweede, en dat is in ieder geval de te gebruiken methode als directe meting van de gradientstroom niet mogelijk is. De orde en de dempingparameters van het gradientspoel-systeem worden bepaald door de impulsresponsie te meten. Omdat fMRI vaak gebruik maakt van zogenaamde EPI-pulsreeksen is de schatting van de akoestische response op een EPI-pulsreeks een nuttige test van de bruibaarheid van de methode. We voorspelden voor de EPI-pulsreeks en geluidsniveau van 104 dB (SPL), voor een signaal waar directe meting een waarde van 102 dB (SPL) leverde. Vooralsnog laat de voorspelde geluidsdrukgolfvorm zowel overeenkomsten als verschillen zien met de direct gemeten versie.

In hoofdstuk 3 wordt een methode gepresenteerd om het akoestische lawaai te reduceren, een methode die is gebaseerd op lineaire systeemtheorie: destructieve interferentie van resonantie-frequenties. Omdat de tijdafgeleide van de gradientstroom de fysische bron van MRI-geluid is, geldt voor de standaard trapeziumvorm voor de stroom dat akoestische excitatie optreedt bij de stijgende en dalende flanken van de trapezia. De door van de dalende flank gegenereerde golf is in tegenfase met die van de stijgende flank. Daarom kan door verschuiving van de afstand tussen de flanken een bepaalde frequentie (en diens boventonen) onderdrukt worden. Deze frequentie wordt afgestemd op de sterkste akoestische resonantiefrequentie van het systeem. Dit idee wordt ook gebruikt om een tweede piek te onderdrukken, daarbij gebruik makend van een tweede trapeziumduur. Hiermee werden niveaureducties bereikt van 6 en 10 dB SPL. Toepassing op en EPI-reeks leverde een in het beste geval een reductie van 12 dB op.

Hoofdstuk 4 richt zich op een kwantittatieve aanpak van de luidheidsreductie. Daartoe worden fysische en subjectieve metingen gedaan aan scannergeluid. In een psychofysisch experiment wordt de luidheid van het EPI-geluid gelijkgesteld aan de luidheid van een tertsband roze ruis, gecentreerd om 1 kHz. Ook werden de 3 componenten van het EPI-geluid, veroorzaakt door de x-, y-, en z-spoelen, afzonderlijk bemeten. In 9 normaalhorende proefpersonen werd gevonden dat de sterkte van het EPI-geluid minder dan lineair toeneemt met het fysische sterkte van de akoestische EPI-signalen. Dit onderstreept onze werkhypothese dat, zolang de relatie tussen fysische stimulus en subjectief percept niet volledig is begrepen, beide eigenschappen moeten worden geanalyseerd.

Hoofdstuk 5 behandelt het gedrag van een MRI-systeem in een praktijkomgeving. Akoestische metingen werden gedaan in 6 punten, binnen en buiten de kern van de scanner. We wilden kwalitatieve en kwantitatieve effecten van de positie en omgeving op de overdracht onderzoeken. Daartoe werden resonantiefrequenties en nagalmtijdconstanten op een aantal verschillende posities gemeten. De resonantie-pieken voor de verschillende gradientspoelen worden op alle locaties gevonden. De x- en y-gradientspoelen tonen maxima bij 648 Hz en 1073 Hz. Deze komen overeen met de banaanvorm-mode van de trillende cylinder. De z-richting-spoelen geven pieken bij 1274

Hz en 1554 Hz, hetgeeen wijst op kegelvormige trillingsmodes van de cylinder. De nagalmtijd van het geheel, en de vorm van de electroakoestische overdrachtsfunctie per spoel zijn vergelijkbaar in alle richtingen. Dit geeft aan dat de ruimteeffecten in dit geval betrekkelijk gering zijn.

Hoofdstuk 6 bespreekt het perspectief voor toekomstige verbetering. De traditionele trend, waarin een toename van hoofdveldsterkte en snellere gradientpatronen van belang lijken, doet er goed aan alle bestaande technieken van lawaaionderdrukking te combineren om tot een redelijk geluidsniveau te komen. De alternatieve trend (microTesla imaging) komt nog slechts op zeer beperkte laboratoriumschaal voor, en is wat behaalde beeldkwaliteit en snelheid vooralsnog niet competatief, maar het lost het lawaaiprobleem eenvoudigweg principieel op.

CHAPTER VII.

CONCLUSIONS AND PERSPECTIVES

ACOUSTIC fMRI NOISE: LINEAR TIME INVARIANT SYSTEM MODEL

The linear time invariant electro-acoustical system approach for our 3T MRI scanner enables appropriate transfer function estimation for each gradient coil. This was demonstrated through reconstruction of the impulse responses from direct measurements of the acoustic responses to sufficiently short current pulses. We used two input specifications: (1) a theoretical gradient waveform calculated by the scanner software, and (2) an experimental recording of the gradient current. The calculated transfer functions for both input specifications are shown to be almost identical up to 4 kHz. It is noted that the step of measuring and recording gradient coils requires availability of recording tools and involves time for the calibration. Thus, the first method is encouraged when a fast and 'standard' gradient coil system characterization is desirable, and when direct measurements of gradient currents are not possible. When analyzing the measured resonances to short pulses we noted that similar resonance modes were excited in the X and Y gradient coils (based on the four main peaks). Such modes arise either as mechanical vibration modes of the cylinder, or as acoustic resonances in the cylinder space acting as a reverberation chamber. It is known that the size and shape of the X and Y gradient coils are similar to each other. Therefore, this result was not unexpected. The electro-acoustical system (per gradient coil) for this scanner can be approximated by a superposition of third order linear systems with impulse responses: $\alpha_i t e^{-t/\tau} \Sigma_i \sin(2\pi f_i t)$ for the major spectral peaks. The time constant τ was found to be approximately 1/100 s, independent of the coil direction, which implies that its reciprocal value the damping factor is estimated to be in the 100 s^{-1} range. The Fourier transforms of the impulse responses provide the complex (or amplitude and phase) transfer functions. These allow the computation of the acoustic response to any given pulse sequence. This is demonstrated for a specific EPI sequence. Currently, the method can predict the shape and overall spectral

energy content of the measured EPI sequence signal within 2 dB. EPI waveform prediction is an added value of this approach, and its further improvements can be applied in MRI acoustic noise control techniques. For the analyzed 3T scanner we find that the measured echo planar imaging amplitude spectrum can be interpreted as a superposition of harmonic, non harmonic and broad band components. The acquisition time per slice (approximately 53 ms) also appears in the acoustic generated EPI waveform. It is reflected in the predicted and measured EPI spectra as constant distance (19 Hz approximately) between frequency peaks. High amplitude EPI noise is very common above 3 kHz but not often reported or discussed in the literature. However, this analysis is relevant because the normal human auditory sensitivity has a maximum at about 3 kHz and extends up to 20 kHz. It has been shown for the examined MR scanner that the acoustic response of the gradient coil system is proportional to the time derivative of the input gradient current. This interpretation supports the results by Hennel et al. which suggest that optimal noise reduction is achieved by optimizing the ramps of the gradient currents; and if combined with other noise reduction techniques should lead to quieter MR scanner sequences. Some studies have shown that acoustic noise during few fMRI studies affects brain activation. It is, however, not clear to which extent MRI acoustic noise affects the results in all fMRI studies of subject performance. This warrants further study of the subjective consequences, in parallel with the development of quieter MR scanners.

MRI ACOUSTIC NOISE REDUCTION BY DESTRUCTIVE INTERFERENCE OF RESONANCE FREQUENCIES

A 3T MR electro-acoustical transfer function is determined by measuring a slightly different input specification shown to be related to the traditional one by a simple mathematical relation. This new transfer function (referred in chapters I, II, III and the summary is estimated using the derivative of the input current) falls of for higher frequencies as expected for a physical system. Our experiments including the first order Lorentz forces physical model have shown the correctness to treat the time derivative of the gradient current as the physical cause of the acoustic noise. The advantage of this new interpretation is exploited in pulse sequence optimization for MRI acoustic noise reduction. That is, an MRI noise reduction technique

based on destructive interference of resonance frequencies is presented and proposed to reinforce the silent pulses concepts while attaining further reduction gains. For isolated pulse shapes the sound pressure spectrum can be optimized to cancel out main resonance frequencies in the transfer function. A single trapezoid of 1ms approximate duration cancels the main resonance frequency of our facility (1045 Hz). The two trapezoid shape of 2.92 ms approximate duration reduced the three main resonance frequencies 625 Hz, (to a lesser extent) 1045 Hz and 1300 Hz. This leads to a reduction in overall sound pressure level (SPL) of maximum 6 dB for the two trapezoid shape with respect to a trapezoid reference. The same resonance frequencies are completely eliminated by constructing a longer trapezoid pulse (2.6 ms) achieving a reduction of 10 dB SPL relative to a trapezoid reference. For shorter durations (less than 1.5 ms), no advantage in the use of sinusoidal pulse shapes is observed in our study. For longer durations, sinusoidal pulse shapes reduce the sound pressure level relative to the trapezoid. Creating a pulse train out of the optimal two trapezoid shape does not lead to a higher reduction in sound pressure level in our MR scanner. The pulse train fundamental frequency becomes a dominant factor; a large difference in sound pressure level is observed when the pulse train fundamental frequency matches a minimum and then a maximum of the transfer function. This pulse train reduces the SPL 12 dB as compared to the trapezoid pulse train and 6 dB SPL as compared to a triangle pulse train. The approach of pulse shape optimization described here can be easily implemented in any facility (using all gradient coil directions X, Y and Z) counting on total sound pressure level reduction. If the MRI gradient coil resonance frequencies could be increased, the duration of our optimized pulse shapes would be very useful for fast sequences, since for this reduction method the pulse time length is inversely proportional to the scanner main resonance frequency (to eliminate). Additional research could explore further MRI noise reduction gains by adding this technique to current noise reduction strategies.

SUBJECTIVE LOUDNESS MEASURE OF fMRI ACOUSTIC NOISE

Typical fMRI acoustic noise has a very special time waveform characteristics such as its impulsive nature and amplitude modulated carrier. Those characteristics suggest a possible influence of basilar membrane nonlinearity on its loudness perception. It is possible that

the loudness perception of fMRI noise with the same rms level but with different peak levels is not equal, since their effective excitation levels would differ after the movement of the basilar membrane (when loud MRI sound is perceived) ends. Also, the variation of the basilar membrane movement with overall level could affect the loudness of modulated sounds such as fMRI noise. Damping effects seems to play a role in loudness perception of fMRI acoustic noise; this suggests that in addition to the total amount of energy in this type of stimuli, it matters how the energy is distributed over time. Noise signatures with lower damping factors and less separated to each other are perceived louder than noise signatures with similar amount of energy but abruptly distributed, that is, displaying a more impulsive nature with higher damping effects. Therefore, fMRI sequences with suppressed frequency components in the 2.5-6 kHz range and highly impulsive nature distributed over a longer time should be preferred over more continuous noise signatures with less damping effects presenting frequency components in the range of ear maximum sensitivity. It is desirable for decreasing fMRI loudness perception to distribute the stimulus energy over a longer period by increasing as much as possible the time selection per slice. In addition, gradient coil systems should place its resonance frequencies in the ear low sensitivity regions. Further research should be carried out to estimate the loudness percept using different fMRI sequences from different facilities.

SOUND ENCLOSURE EFFECTS IN MRI ACOUSTIC CHARACTERIZATION

Electro-acoustical characterization of one magnetic resonance imaging (MRI) gradient coil system was studied in six different locations inside and outside the scanner bore. The same two main resonance frequencies per coil are found to be maxima at all six transfer function gain locations. Across different coils, the X and Y direction present common transfer function gain maxima around 648 Hz (mean value) and 1073 Hz (mean value). The former is expected to represent the so called banana-shape (transversal) mode of the vibrating structure. The Z direction coil presents transfer function gain maxima around 1274 Hz and 1554 Hz. The former (1274 Hz) is expected to represent the so called cone-shape (radial) mode of the vibrating structure. The overall reverberation time (in the order of 200 ms) and electro-acoustical transfer function shape per coil is to some extent comparable in all

locations. Minor differences are due to signal to noise ratio and time delays associated to locations far away (outside MRI bore) from noise source. These findings suggest a minimum MRI bore enclosure effect in electro-acoustical transfer function estimation for our facility. However, further research on MRI acoustic noise characterization should include estimation of enclosure effects parameters such as reverberation time per frequency inside and outside the MRI.

FUTURE PERSPECTIVES

MRI acoustic noise generation is expected to be for the next couple of years a serious concern because it reaches safety limits in many cases; in order to effectively reduce this noise, a stronger multidisciplinary approach must be followed between hospital community (including patients), audiologists, industry and academia researchers. Finding an ultimate noise reduction technique is not straightforward; every magnetic resonance (MR) scanner has its own acoustic transfer function characteristics and personalized sequences depending on its own software parameters. Although, electro-acoustical MRI transfer function characterization combined with optimum sequence programming is very economical and effective in significantly reducing the MRI generated acoustic noise; in order to obtain a large reduction in MRI acoustic noise generation for existing scanners, an appropriate combination of different noise reduction techniques should be implemented to a great extent. Techniques such as optimized pulse sequences, insertion of acoustic absorbing materials, new gradient coil designs, active vibration control and vacuum vessel enclosure (if possible) should be applied to the same MRI scanner facility. This should lead to a large reduction in generated acoustic noise.

However, higher field MRI encounters other disadvantage that is, peripheral nerve stimulation due to electrical currents generated by the fluctuating MRI magnetic field. In addition, it is somewhat unclear to properly foresee the safety of constant magnetic fields of approximately 10000 times higher in magnitude than the average earth magnetic field; since this would be based only on current biomedical sensor technology and accepted human physiology theories. This current knowledge limitation leaves a great opportunity for the emerging technique of (Superconducting Quantum Interference Device) SQUID-detected MRI in microtesla fields, which proposes a

less unnatural magnetic field strength in the same order of magnitude of the earth magnetic field. Therefore, this emerging system is expected to be many orders of magnitude (in theory approximately 80 dB) more silent compared to higher field MRI systems. This evolving technique also promises reduced costs, more portability and broader coverage for patients, since preliminary results suggest that microtesla MRI could be used to obtain undistorted images in the presence of metallic implants or biopsy needles. In contrast to high field MRI images which are often distorted in the presence of a piece of metal. Moreover, SQUID-detected MRI in microtesla fields (if it evolves successfully) could offer an additional advantage by fusing MRI with magneto encephalography (MEG) for simultaneous MEG-MRI, since they both share same SQUID sensor technology.

Therefore, in the long term future the golden decade's hegemony of higher field MRI is uncertain, just like the strong need for acoustic noise reduction. It might be possible that emerging ultra low and high field MRI could coexist. But, in the long term future the costs benefit ratio, the technique suitability, sustainability and its well documented safety would drive MRI popularity towards lower magnetic fields, making higher field MRI systems usable for few institutions with very high amounts of money and only for few research purposes. Thus, a possible future scenario is the slowly but steady development of ultra low field MRI techniques. This could come together with the development of emerging photo-(thermo) acoustic imaging techniques to be used in anatomical and functional human studies of the brain and other tissues. The health industry could receive much benefit by supporting the research and development of these new emerging technologies that promise to be more natural, quiet, less expensive, friendlier and with broader coverage for patients.

ACKNOWLEDGEMENTS

Special gratitude goes to that huge part of humankind who has supported me with the research and writing of this thesis. Since us humans are all related, by thanking seven persons it will imply thanking the whole everyone system (by resonance). Those fantastic seven are my advisor Diek, our ex-scientific coordinator Britta, the athlete scientist Umut, the sharp artist Isa, the “inigualable e inconfundible” Jeske Uitterhoeve, the research BCN-RUG joint Tinie A-Diana K-Annette Korringa-Mbemba J-Primoz P-Anneke Toxopeus-Tofanio-Meltem-Monika Z-Monica D-Marc-Idilia-Johan-Christiaan-Ramona-Marjolijn-Martijn-Luca-Richard J-Marco G-Joyce and last but not least my officemates super combo special (Gerke, Lav, Sony, Cris, Dave, Erik, Rick and Bran). Now, the majestic 12 which I owe lots of support and encouragement are Juan C, Martha C, Fidias L, Mark L, Daniela D, Diego C, Dorian C, Flor V, Yezid T, Rob V, Edmanuel T, Leonardo A; and of course lots of gratitude to my parents, brothers, sister and relatives. Finally, thanks to all those people that I have not forgotten but for whom this thesis just proves a bit too short.

Thanks to the city of Groningen for offering such a wonderful mixture of foreign human beings, languages, cultures and of course lots of water and darkness. Living and studying abroad can be one of the most challenging experiences, but at the same time one of the most rewarding. I will never forget so many PhD scientific trips, courses and meetings all over the world that I had the pleasure to attend. Dr. Elaine Aron, thanks a lot for your outstanding gift (book) to society.

“What it does not kill you, for sure it will make you stronger or fat (joke). Porque no hay mal que dure 100 años ni cuerpo que lo resista, plop.”